

## Article

# In Situ Monazite U–Pb Ages in Thin Sections from the Giant Bayan Obo Fe–REE–Nb Deposit, Inner Mongolia: Implications for Formation Sequences

Pengfei Tian <sup>1,2</sup> , Xiaoyong Yang <sup>2,3,\*</sup>, Yulun Xiao <sup>3</sup>, Wanming Yuan <sup>4</sup> and Zifei He <sup>1</sup>

<sup>1</sup> The Cultivation Base of Shanxi Key Laboratory of Mining Area Ecological Restoration and Solid Wastes Utilization, Shanxi Institute of Technology, Yangquan 045000, China

<sup>2</sup> Ganjiang Innovation Academy, Chinese Academy of Sciences, Ganzhou 341000, China

<sup>3</sup> School of Earth and Space Sciences, University of Science and Technology of China, Hefei 230026, China

<sup>4</sup> Institute of Earth Sciences, China University of Geosciences, Beijing 100083, China

\* Correspondence: xyyang@ustc.edu.cn

**Abstract:** The Bayan Obo deposit is the largest REE resource in the world. Although many isotopic dating methods have been applied, ages based on petrography and closure temperatures still lack discussion. In this study, three digital petrographic images were created based on full-scanning microscopy, BSE, and TESCAN integrated mineral analysis (TIMA), providing a more scientific method for analyzing the mineral types, distributions, and content of the Bayan Obo deposit. By combining the full-scan images, monazites were selected in thin sections and dated in situ. The monazite in the body ores sample yields three <sup>207</sup>Pb intercept ages of 657 ± 25 Ma (MSWD = 1.06), 763 ± 16 Ma (MSWD = 1.3), and 689 ± 22 Ma (MSWD = 8.1), and the monazite in one section yields maximum and minimum ages of 1393 ± 142 Ma and 429 ± 24 Ma, respectively. Combined with previous studies, the earliest and major stages of carbonatites, REE, and dikes in the Bayan Obo deposit area were dated at ~1.4 Ga and ~1.3 Ga, respectively. Due to the multiple subduction and accretion events related to the Paleo-Asian Ocean and North China Craton, the Bayan Obo deposit is intensely overprinted, with a tectonic-thermal event recorded at ~1.0–0.2 Ga. The multiple or protracted isotopic ~1.4–0.4 Ga ages in the Bayan Obo deposit account for five reasons. First, the separate thermal events and the partial recrystallization of monazite. Second, the diffusion of daughter products from the host mineral over time. Third, differences in the closure temperatures of different minerals and isotopic chronologies. Four, resetting of the closure system due to high temperature and hydrothermal alteration. Five, the minerals and transformed ores that formed in the Paleozoic. The in situ monazite U–Pb ages in thin sections provide insight into formation sequences from the giant Bayan Obo Fe–REE–Nb deposit.

**Keywords:** Bayan Obo; monazite; TIMA; closure temperature; North China Craton (NCC)



**Citation:** Tian, P.; Yang, X.; Xiao, Y.; Yuan, W.; He, Z. In Situ Monazite U–Pb Ages in Thin Sections from the Giant Bayan Obo Fe–REE–Nb Deposit, Inner Mongolia: Implications for Formation Sequences. *Minerals* **2022**, *12*, 1237. <https://doi.org/10.3390/min12101237>

Academic Editor: Yasushi Watanabe

Received: 29 August 2022

Accepted: 26 September 2022

Published: 28 September 2022

**Publisher's Note:** MDPI stays neutral with regard to jurisdictional claims in published maps and institutional affiliations.



**Copyright:** © 2022 by the authors. Licensee MDPI, Basel, Switzerland. This article is an open access article distributed under the terms and conditions of the Creative Commons Attribution (CC BY) license (<https://creativecommons.org/licenses/by/4.0/>).

## 1. Introduction

China is the world's largest producer of REE in terms of reserves and production. According to the USGS, China has 42% of the world's REE reserves, and Chinese REE production accounted for 86% of the total world production in 2014. More than 80% of China's LREE resources are distributed in the Bayan Obo region of Inner Mongolia in northern China [1,2].

To better determine the formation processes of the giant Fe–REE–Nb deposit of Bayan Obo, metallogenic ages have always been emphasized. Geochronological data from U–Th–Pb, Sm–Nd, Rb–Sr, K–Ar, Ar–Ar, Re–Os, and fission track methods show a wide range of ages, ranging from 2.5 Ga to 0.05 Ga [1,3–12]. There are three main opinions regarding the age of the mineralization of Bayan Obo REE, with estimates ranging from 1.4 Ga Ma to

0.4 Ga: (1) mineralization was in the Middle Proterozoic, (2) Caledonian mineralization, and (3) the existence of multi-phase mineralization [5,13,14].

The ages reported for the Bayan Obo deposit that are determined by different studies using the same method vary widely. This is mainly due to mineral assemblage and whole-rock dating showing different age characteristics (two or more age groups), which not only occurs for different minerals analyzed using the same method (such as Sm–Nd ages ranging from ~1.8 Ga to ~0.4 Ga) but also for the same mineral analyzed using different methods (e.g., Th–Pb and Sm–Nd ages of monazite and bastnaesite range from ~1.3 Ga to ~0.2 Ga).

Researchers often compare the ages of different methods together. Are the corresponding minerals of Th–Pb, Sm–Nd, and other chronological dating methods consistent and comparable? Can dating of the whole rock or mineral assemblages represent the age of REE metallogenesis? To answer these questions, three fundamentals require more consideration. (1) Checking that the ores described by different studies are the same: There are over 100 mineral species in the Bayan Obo deposit, and the ores produced by the combination of different minerals are even more diverse. Different strategies may have been used to sample and describe the same rock. Therefore, it is important to create optical panoramic scans and digital panoramic maps of mineral phases to analyze rock sections. (2) The standardization of age statistics: If individual minerals or assemblage minerals have large age differences (e.g., monazite, bastnaesite, and apatite in this study), the intercept age determined by random points will be different even if the obtained ages of minerals are determined in situ over small distances (~500  $\mu\text{m}$ ). This is because the age calculation itself is a statistical process, and ~30–50 points are routinely used to form the intercept age. If the age difference in a small area is large, there will theoretically be different intercept ages in multiple test groups. In this case, it is necessary to analyze the relationship between the age of a single point and the petrography [6,7,10–12]. (3) Different closure temperature: The closure temperatures of zircon U–Pb, monazite U–Pb, muscovite Rb–Sr, biotite Rb–Sr, biotite  $^{40}\text{Ar}/^{39}\text{Ar}$ , and apatite fission track are  $800 \pm 50$  °C,  $710 \pm 30$  °C,  $390 \pm 110$  °C,  $330 \pm 40$  °C,  $290 \pm 40$  °C, and ~110 °C, respectively [15]. According to Danišik [16], the sensitive temperatures of zircon U–Pb and monazite U–Pb are 770–1100 °C and 840–1020 °C, respectively. Liu et al. [17] calculated the Pb closure temperature using the diffusion coefficient of Smith and Giletti [18] and the parameters of Cherniak et al. [19], which are ~600–800 °C and ~1000 °C, respectively. Although there are differences in the closure temperatures of the same mineral between the different studies, comparisons of the differences between the closure temperatures of different minerals are the same. In the monazite dating system, dynamic recrystallization during deformation can reset isotopic systems below nominal closure temperatures, as well as coupled dissolution-reprecipitation during hydrothermal alteration [20].

For the Bayan Obo deposit, if the older age is constrained by the younger age, for example, the zircon U–Pb age from the slate ( $518.8 \pm 7.5$  Ma) [21] that covers the host dolomite, and if the thermal events represented by this age generally affect the slate, does it mean that systems with a closure temperature lower than  $800 \pm 50$  °C have been reset? However, the large number of ~1.3 Ga Sm–Nd ages and ~1.0–0.4 Ga Th–Pb ages [6] suggest that the ~0.5 Ga thermal event affecting the slate is a local event. If the ~0.5 Ga thermal event is universal, all rocks in the region will experience a high temperature of  $800 \pm 50$  °C, the lower closure temperature system will be reset, and all ages should be <0.5 Ga, which is inconsistent with the facts. Therefore, the ~0.5 Ga thermal event was localized; otherwise, the in situ Th–Pb age of monazite would not be younger than the whole-rock Sm–Nd age.

To better constrain the REE mineralization processes that formed the Bayan Obo deposit, full optical, TESCAN integrated mineral analyzer (TIMA), and back-scatter election (BSE) scans were performed for sections of the ore-hosting dolomites to establish accurate panoramic digital petrographic maps. The monazites in each section were selected based on digital petrographic maps for in situ dating and to analyze the relationship between age and petrography. We hope the experimental process combined with the full optical, TIMA,

and situ dating will give more scholars some instructions. Another objective of this study is to propose an age sequence of the Bayan Obo deposit using data from the current study and previous studies.

## 2. Geological Setting

### Ore Geology

The Bayan Obo Fe–REE–Nb deposit is located on the northern margin of the North China Craton (NCC) [22]. The NCC is bordered by the Central Asian Orogenic Belt to the north, and the two units are separated by the Ulanbaolige deep fault [2,23] (Figure 1a,b). The east–west extension of the Ulanbaolige–Kuanggou Fault intersects with the Ulanbolig Fault, and at the intersection is the dolomite carbonate body of the giant Bayan Obo deposit [24]. On the northern and southern sides of the Baiyinjiolake–Kuanggou fault, there are vertical or oblique fractures that converge to form a giant tectonic fracture system playing a significant role in the tectonic, magmatic, and mineralization processes in the area (Figure 1c). The Kuanggou fault on the northern side of the Bayan Obo deposit is well-exposed and is a reverse fault that dips 75° to the south.

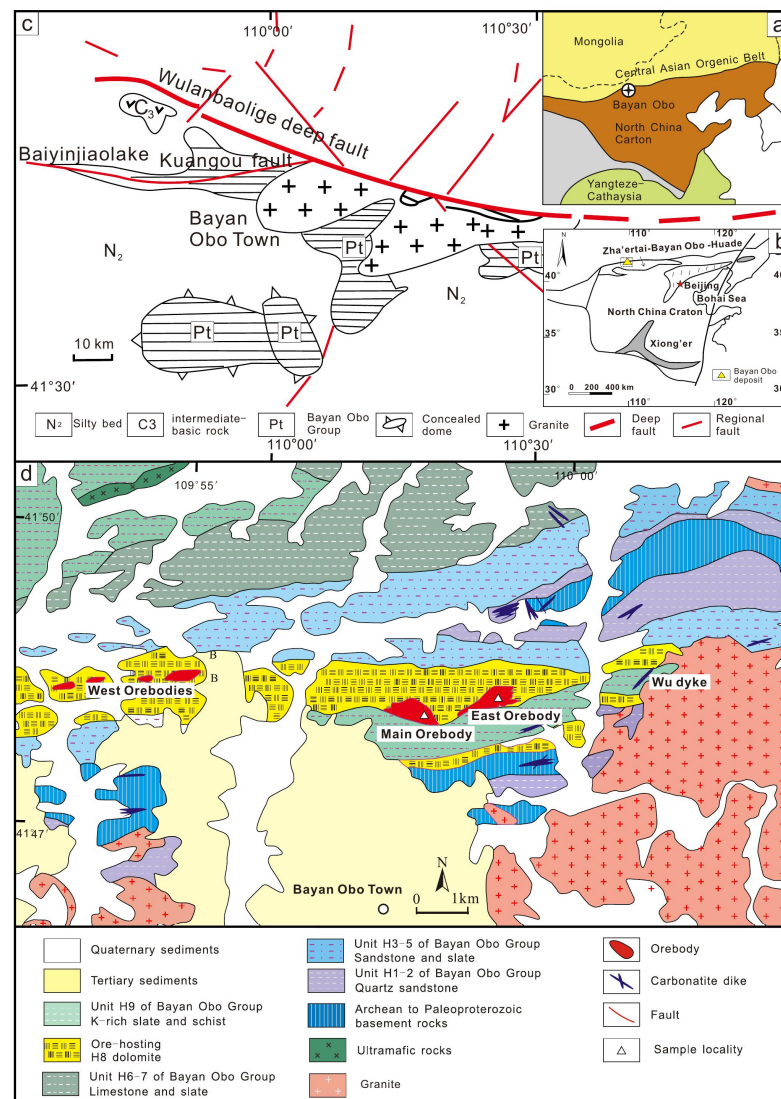


**Figure 1.** Location and stratigraphy of the Bayan Obo deposit. (a) The tectonic location in the North China Craton (modified from [25]); (b) geological map of the North China Craton (modified from [26]); (c) regional structural geological map of the Bayan Obo region (modified from [2]); (d) geological map of the Bayan Obo deposit and surrounding area (modified from [8]).

The main exposed strata in the Bayan Obo mining area are from the Middle Proterozoic Bayan Obo Group. The Lower Proterozoic strata are mainly exposed along the anticline axis and are rare. Only a small amount of post-Paleozoic strata is exposed in the northeast of the mining area. The Bayan Obo Group has an east–west length of ~480 km and a total thickness of ~10990 m [24]. It can be divided into 18 horizons, including lower (H1–H10) and upper (H11–H18) horizons, and comprises six formations, including the Dulahala (H1–H3), Jianshan (H4–H5), Halahuogete (H6–H8), Bilute (H9–H10), Baiyinbaolage (H11–H12), and Hujiertu (H13–H18) formations [24] (Figure 1d). The depositional age of H8 was determined to be between ~1710 and 1447 Ma by the U–Pb ages of detrital zircons from H7 [27] and the Re–Os geochronology of the black schist from H9 [28], respectively.

The Fe–Nb–REE deposit is mainly concentrated in the H8 dolomite of the Bayan Obo Group. The REE–Nb–Fe ores in the main and eastern ore bodies of the Bayan Obo deposit can be divided into six types: banded, massive, dolomite, riebeckite, biotite, and aegirine [24].

### 3. Samples

According to grain size, monazite in the Bayan Obo deposits can be divided into fine-grained and coarse-grained. The fine-grained monazite is generally euhedral to subhedral, translucent, ~20 µm in diameter, and is distributed as aggregates in the dolomite ores (sample D-1) or in strips in aegirine ores. The coarse-grained monazite is generally subhedral, translucent, ~200–600 µm in diameter, and is mainly distributed in pyrite ores associated with biotite, aegirine, and aegirine augite without dolomite (samples Fe-1 and B-2).

Sample D-1 is a gray dolomite rock. The mineral composition of D-1 was ankerite (88.02%), fluorite (5.01%), monazite (1.63%), bastnaesite (1.04%), quartz (0.94%), hematite/magnetite (0.63%), dolomite (0.44%), baryte (0.16%), pyrite (0.11%), and pyrrhotite (0.07%). Monazite occurs as single ~20 µm particle with a polycrystalline distribution (Figure 2). Bastnaesite and monazite often assemble together and are difficult to distinguish under BSE (Figure 3). Fluorite and quartz are the main components of the fine veins (Figure 2).

The mineral composition of Fe-1 includes biotite (31.56%), aegirine (21.63%), siderite (9.93%), magnesio-riebeckite (9.35%), hematite/magnetite (6.09%), orthoclase (3.65%), quartz (2.25%), apatite (0.81%), and monazite (0.67%) (Figure 4). Aegirine does not show typical green stripes but is black, mixed with biotite and apatite (Figure 5). Monazite mainly occurs as ~200–600 µm crystals within or at the edge of biotite.

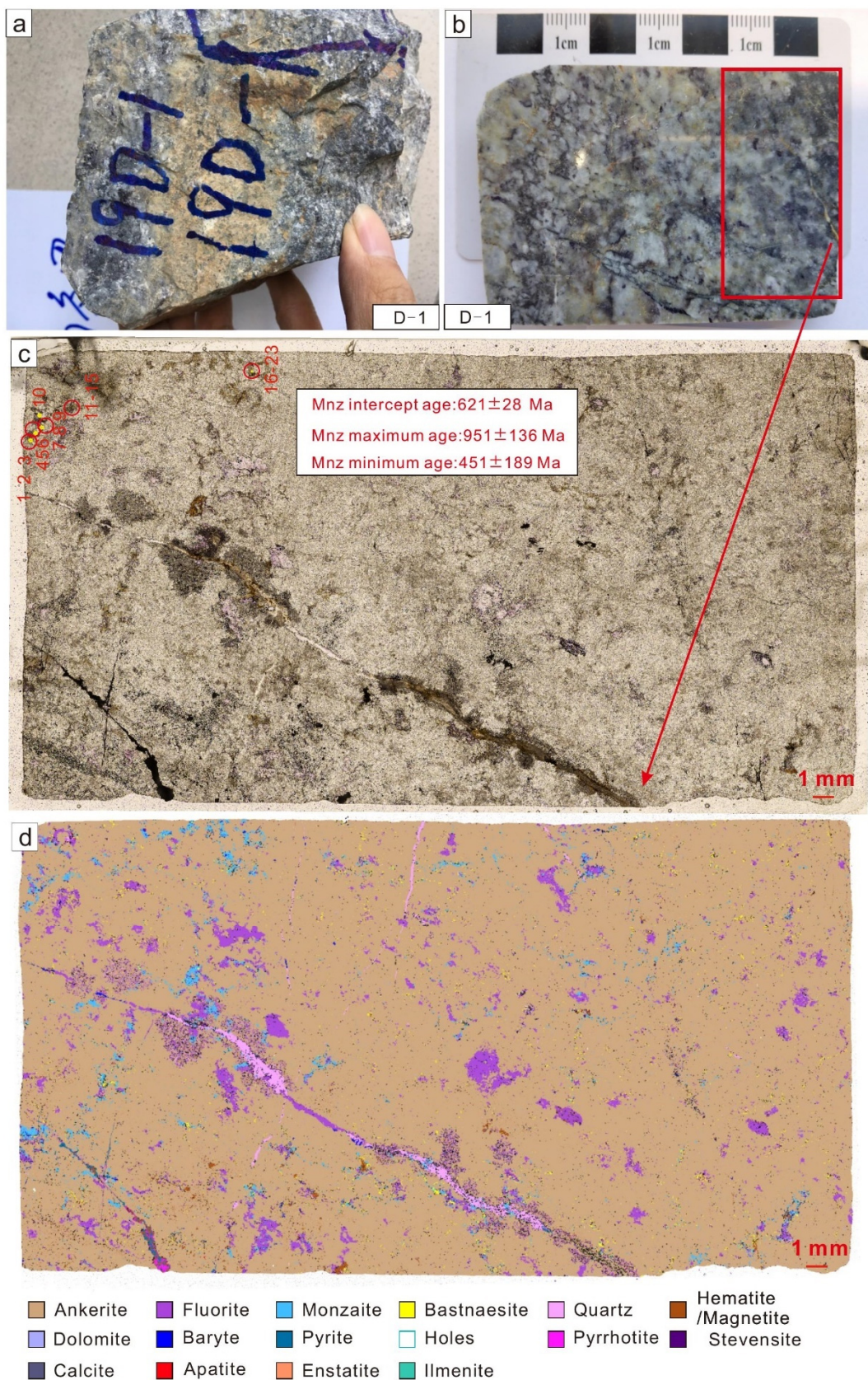


**Figure 2.** The petrological characteristics of sample D-1. (a) Hand specimen; (b) photograph of the polished surface of the sample, (c) panoramic photomicrograph under transmitted light; (d) TIMA mineral maps. The red box in (b) is the location of the thin section of (c).

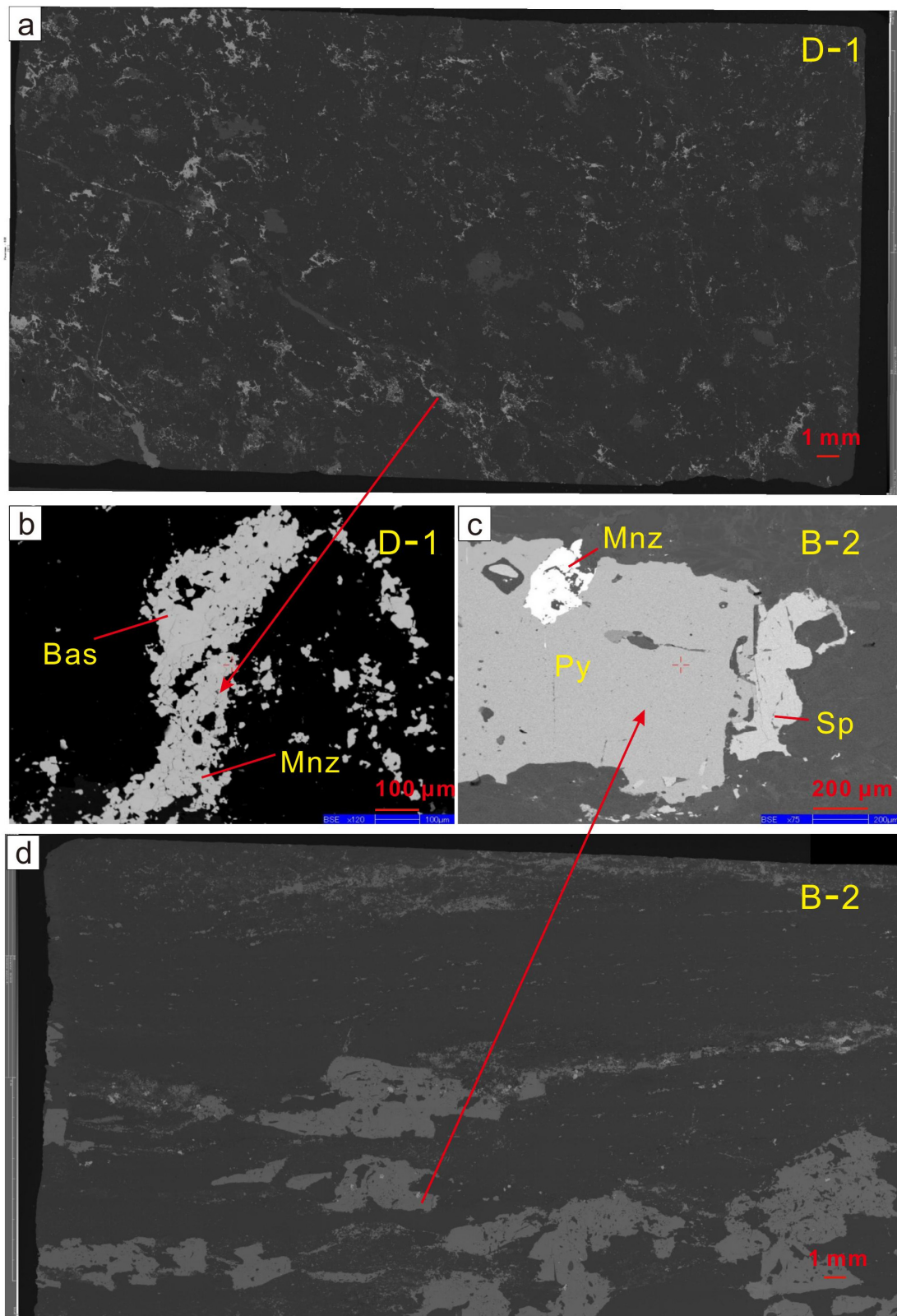


**Figure 3.** Backscattered electron images showing characteristic mineral assemblages and textures observed in the Bayan Obo deposit. (a,d) are whole BSE scans, (b,c) are detail BSE images. Mnz—monazite; Bas—bastnasite; Sp—Sphalerite; Py—Pyrite.

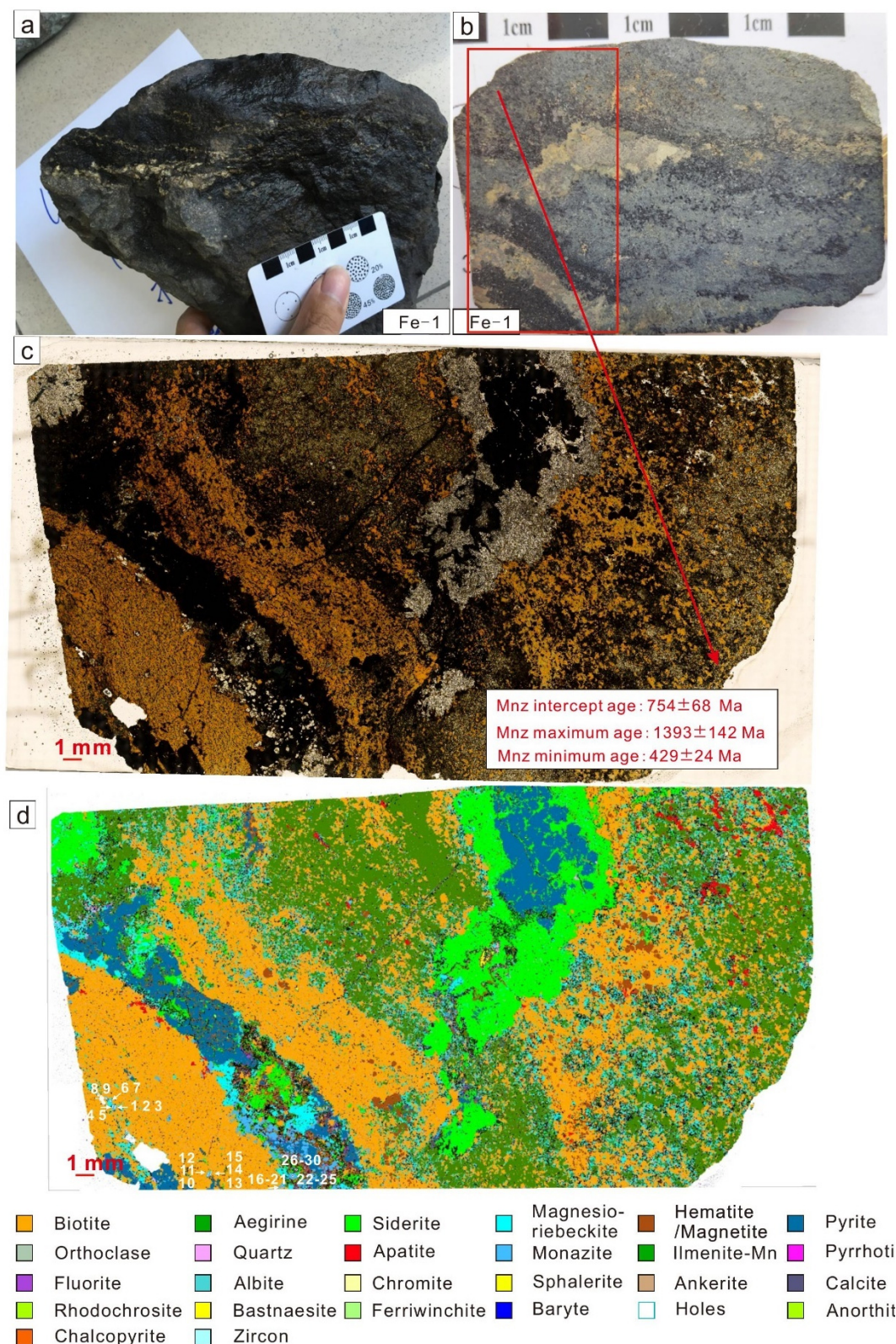


**Figure 4.** The petrological characteristics of sample Fe-1. (a) Hand specimen; (b) photograph of the polished surface of the sample, (c) panoramic photomicrograph under transmitted light; (d) TIMA mineral maps. The red box in (b) is the location of the thin section of (c).

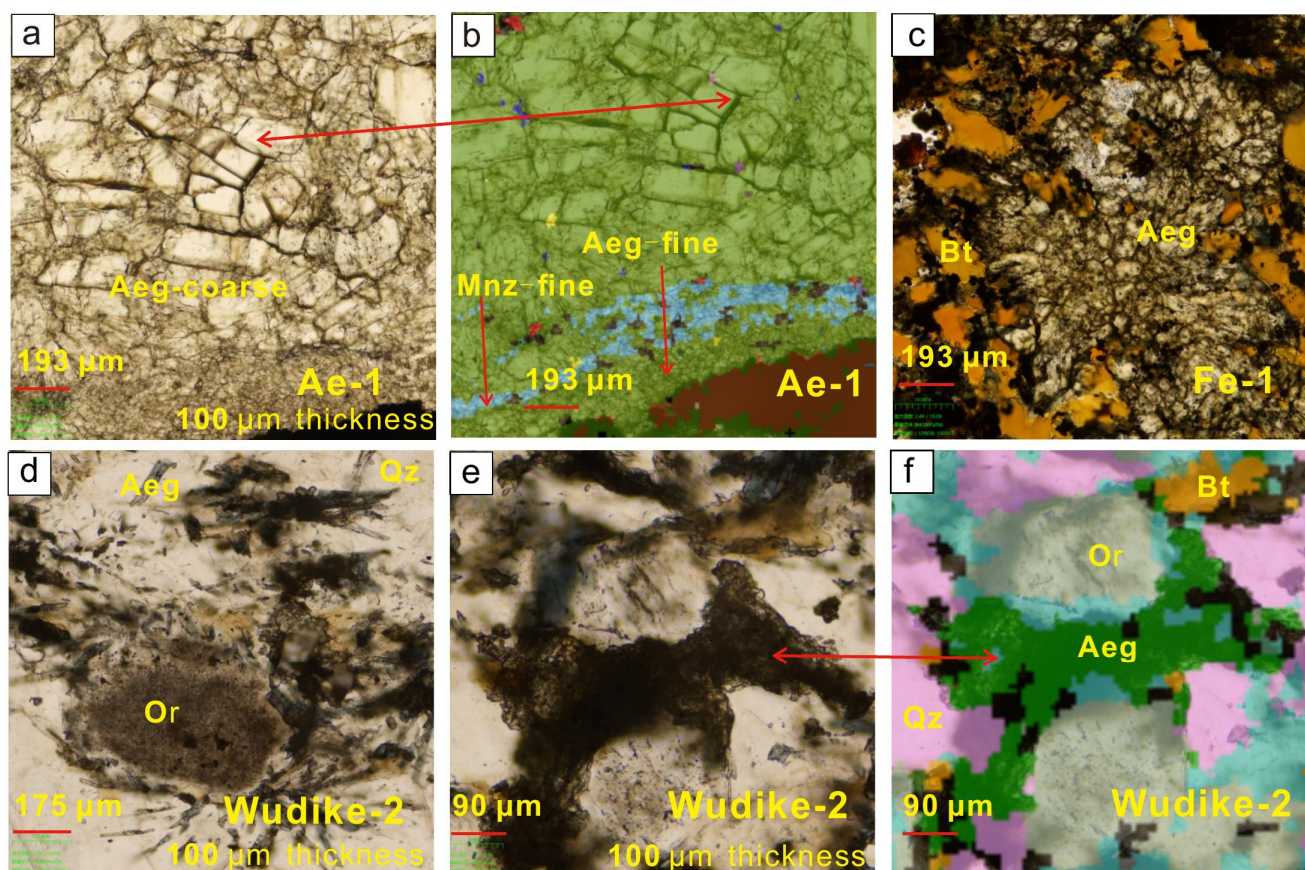


**Figure 5.** The petrological characteristics of aegirine. (a,b) Coarse and fine aegirine are common in green aegirine rock. (c) In the sample Fe-1, aegirine is often distributed with apatite and monazite pyrite, and the aegirine particles are mixed with impurities. (d–f) In Wu dike, aegirine shows acicular characteristics, which is very different from the characteristics of aegirine in the deposit. Aeg—Aegirine; Bt—Biotite; Mnz—monazite; Or—Orthoclase; Qz—Quartz. The mineral composition of B-2 has aegirine-augite (66.86%), pyrite (14.27%), aegirine (5.51%), calcite (3.72%), hematite/magnetite (1.54%), apatite (1.21%), quartz (0.99%), pyrrhotite (0.75%), and monazite (0.20%) (Figure 6). In the Bayan Obo deposit, aegirine-augite occurs in both the aggregate and columnar forms. In the aggregate type, single long (~0.2–1 mm) columnar crystals of aegirine constitute the aggregate, and the rock is dominated by aegirine (Figure 7a–c). Aegirine-augite also occurs as ~1.5 mm-long acicular and columnar forms in orthoclase (Figure 7d–f). Sample B-2 is an aggregate type with pyrite. Monazite occurs as inclusions in aegirine-augite and pyrite (Figure 3c).

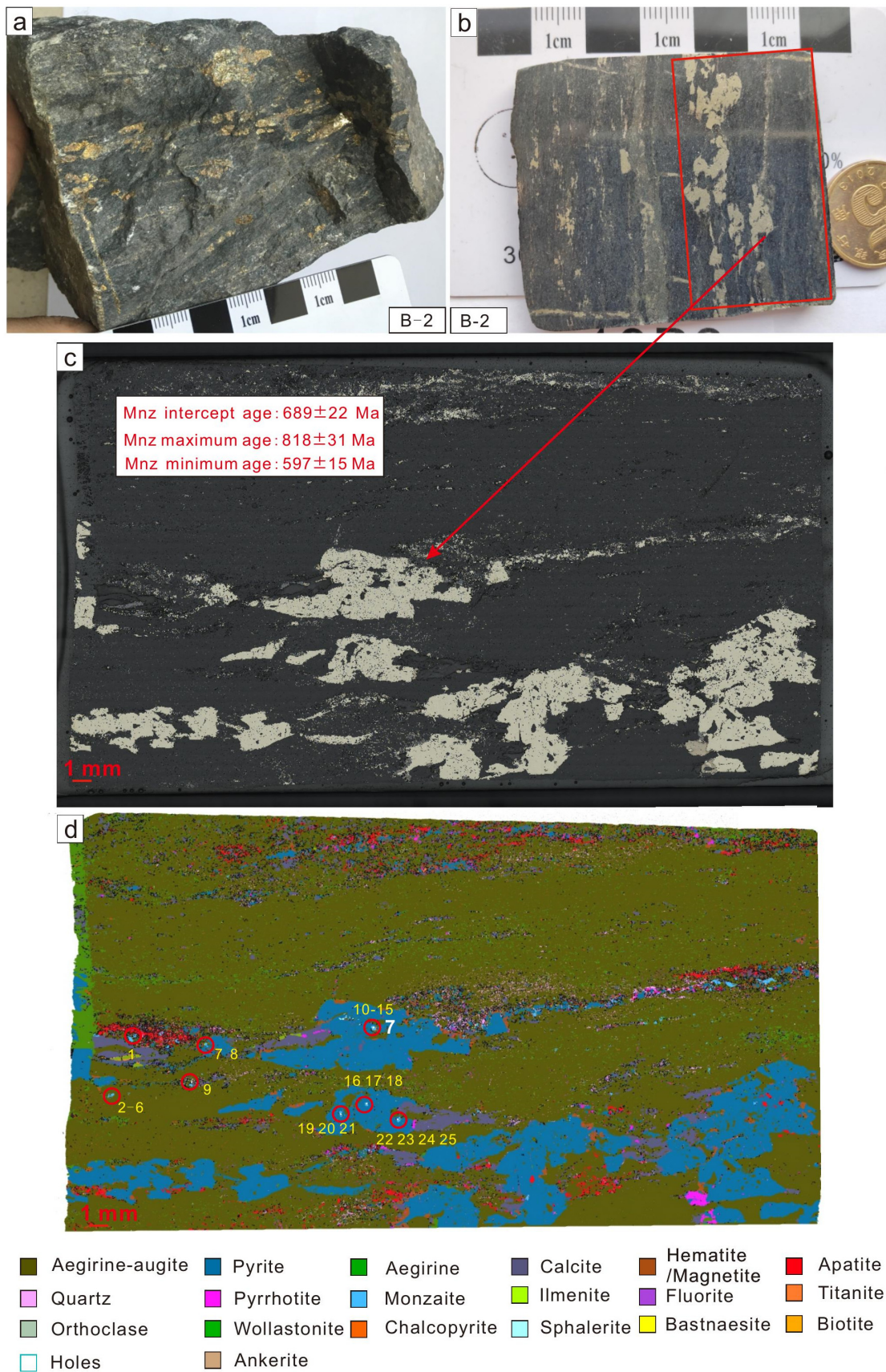


**Figure 6.** The petrological characteristics of sample B-2. (a) Hand specimen; (b) photograph of the polished surface of the sample; (c) panoramic photomicrograph under reflected light; (d) TIMA mineral maps. The red box in (b) is the location of the thin section of (c).

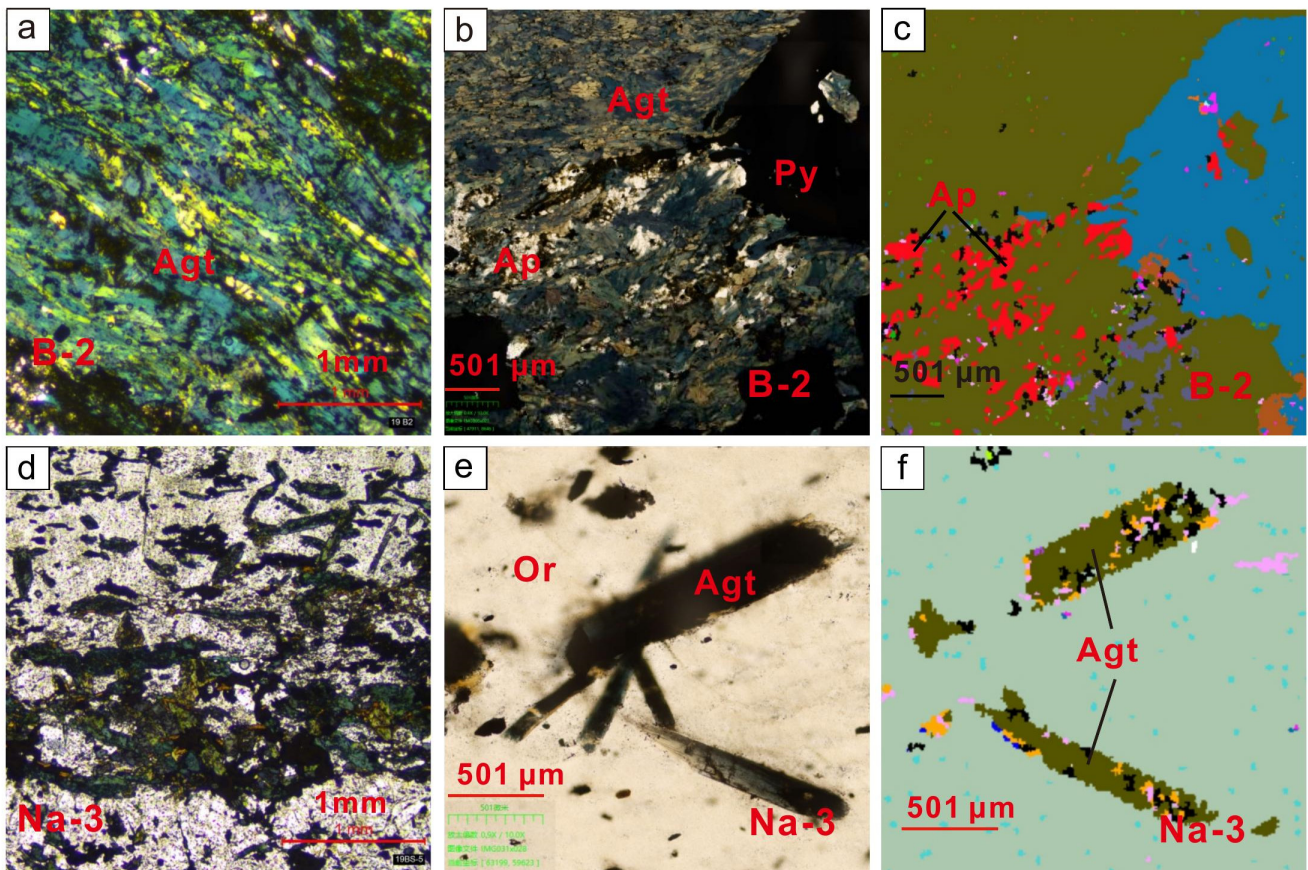


**Figure 7.** Aegirine-augite occurs in both aggregate forms (a–c) and columnar forms (d–f). Agt—Aegirine-augite; Ap—Biotite; Or—Orthoclase; Py—Pyrite.

#### 4. Analytical Methods

##### 4.1. Microscope Full Scan

Full scanning of the rock's thin section was performed at Langfang Tuoxuan rock and mineral Testing Service Co., Ltd. A panoramic photo was automatically captured by a high-power microscope. A panoramic photo was compiled from ~2500 photos (taking ~500 s). Each panoramic photo was provided with a coordinate system to calibrate the position of the mineral, and the minimum scale reached 2.2  $\mu\text{m}$ . A thin section could produce three type panoramic photos, including the transmitted light, transmitted light + orthogonally polarized light, and reflected light.

##### 4.2. TIMA Method

A modern automated mineralogical approach that was adopted for detailed (either complex or selective) insights into the phase/mineral distribution was used. A TIMA (TESCAN integrated mineral analyzer) housed at the Nanjing Hongchuang Geological Exploration Technology Service Co., Ltd. (Nanjing, China). was used for the liberation analysis of selected rocks. The liberation data were collected with the “dot mapping” mode, which included the collection of BSE and energy dispersive X-ray spectroscopy (EDS) data. At each point, the BSE levels were determined. If the BSE level was above a certain threshold, the beam was directed at this spot until 1000 counts from the spectrometer were collected. An acceleration voltage of 25 kV and probe current of 9 nA were used. The working distance was set to 15 mm. The pixel and dot spacing were set to 3  $\mu\text{m}$  and 9  $\mu\text{m}$ , respectively. The current and BSE signal intensities were calibrated on a platinum Faraday cup using an automated procedure. The EDS performance was checked using a manganese standard.

### 4.3. Monazite U–Pb Dating

U–Pb and trace elements in monazite were measured in situ by LA-ICP-MS at the In Situ Mineral Geochemistry Lab, Ore Deposit and Exploration Center (ODEC), Hefei University of Technology, Hefei, China. Analyses were performed using an Agilent 7900 Quadrupole ICP-MS equipped with a Photon Machine Analyte HE 193-nm ArF excimer laser ablation system. Ablation was performed in an atmosphere of UHP He (0.90 L/min), and upon exiting the cell, the aerosol was mixed with Ar (0.85 L/min) immediately after the ablation cell. The ICP-MS system was optimized daily to maximize sensitivity to isotopic values of the mass range of interest while minimizing molecular oxide species production (i.e.,  $^{232}\text{Th}^{16}\text{O}/^{232}\text{Th}$ ), typically  $< 0.3\%$  [29,30].

Bananeiro [31] and NIST 610 standards were used for external calibration of the U–Pb age and trace element content calculations. Monazite RW-1 [32] was analyzed between each 10 unknown samples for quality control. Each block of 10 unknown samples was bracketed by the analysis of standards. Each analysis started with a blank of 20 s, followed by another analysis time of 40 s after the laser was turned on. A laser beam with a diameter of 20  $\mu\text{m}$  at a repetition rate of 7 Hz and an energy density of 2.5 J/cm<sup>2</sup> was used. The flow rate of the He carrier gas was set at 0.85 L/min. This gas carried the ablated aerosol out of the sample chamber, mixed with Ar gas, and directed to the plasma torch. Offline data processing was performed using ZSkits software (copyright of Yanduzhongshi Geological Analysis Laboratories, Beijing, China), including sample and blank signal selection, drift correction, and conversion of LA-ICP-MS spectra to element concentrations and U–Th–Pb isotopic ratios and ages. Time-dependent drifts of the U–Th–Pb isotopic ratios were corrected by linear interpolation (with time) according to variations in Slyudyanka. The preferred U–Th–Pb isotopic ratios used for the Bananeiro standards were from Gonçalves, Lana, Scholz, Buick, Gerdes, Kamo, Corfu, Marinho, Chaves, and Valeriano [31]. The uncertainty of the preferred values for the external standard RW-1 was applied to the final sample results. For age calculations, a weighted average of the joint Pb-corrected ages was used with a Tera–Wasserburg Concordia intercept age. We obtained the U–Pb age of monazite RW-1 of  $904.12 \pm 2.15$  (N = 6), which is similar to that of Ling et al. [32] ( $904.15 \pm 0.26$  Ma). Concordia plots and weighted mean calculations were performed using Isoplot (Version: 3.0, Kenneth R. Ludwig, Berkeley, CA, USA) [33].

## 5. Results

### Monazite Ages

Monazite in sample D-1 is euhedral and  $\sim 20$   $\mu\text{m}$  in size. Because the laser beam spot size is 20  $\mu\text{m}$ , it is difficult to date a single monazite. Therefore, pure monazite assemblages were selected for analysis; the corrected  $^{207}\text{Pb}$  intercept age was  $621 \pm 28$  Ma (MSWD = 2.1). If a higher deviation age is excluded, the  $^{207}\text{Pb}$  intercept age is  $657 \pm 25$  Ma (MSWD = 1.06). The maximum and minimum ages of the monazite grains were  $951 \pm 136$  Ma and  $451 \pm 189$  Ma, respectively. Thus, the ages of the monazite assemblages varied widely; for example, points 1, 2, and 3 are  $451 \pm 189$  Ma,  $839 \pm 124$  Ma, and  $951 \pm 136$  Ma, respectively, as are points 7, 8, and 9 (Table 1 and Figure 8).

**Table 1.** Monazite U–Pb isotopic data of the sample D-1 from the Bayan Obo deposit.

Sample	$^{207}\text{Pb}/^{206}\text{Pb}$		$^{207}\text{Pb}/^{235}\text{U}$		$^{206}\text{Pb}/^{238}\text{U}$		$^{207}\text{Pb}/^{206}\text{Pb}$		$^{207}\text{Pb}/^{235}\text{U}$		$^{206}\text{Pb}/^{238}\text{U}$		Corrected $^{207}\text{Pb}$	
	Ratios	Error	Ratios	Error	Ratios	Error	Age (Ma)	Error	Age (Ma)	Error	Age (Ma)	Error	Age (Ma)	Error
D-1-1	0.85288	0.02038	151.28601	10.43775	1.27279	0.07046	5012.71	33.89	5103.07	69.59	5292.56	199.84	451	189
D-1-2	0.74446	0.02205	73.47275	4.59344	0.74074	0.04314	4819.02	42.38	4376.74	62.63	3573.33	159.76	839	124
D-1-3	0.65630	0.03403	47.13776	3.06107	0.53915	0.02746	4637.87	74.84	3933.66	64.57	2779.87	114.99	951	136
D-1-6	0.73768	0.03965	56.20797	3.87909	0.60257	0.03811	4805.92	76.95	4108.94	68.85	3040.17	153.28	716	174
D-1-7	0.71520	0.04289	52.86402	5.33199	0.61839	0.05588	4761.56	86.05	4047.79	100.51	3103.50	222.58	832	199
D-1-8	0.74562	0.03310	45.67565	2.42007	0.47810	0.02308	4821.25	63.51	3902.34	52.65	2519.00	100.66	545	116
D-1-9	0.42370	0.01684	10.39226	0.46990	0.18046	0.00508	3995.39	59.44	2470.36	41.88	1069.47	27.74	629	28
D-1-10	0.75448	0.02597	57.35004	2.67765	0.57737	0.02609	4838.13	49.21	4129.01	46.60	2938.01	106.61	618	110
D-1-11	0.62007	0.01960	32.41145	1.74210	0.38467	0.01712	4555.74	45.82	3562.88	52.94	2098.07	79.71	784	63
D-1-12	0.81813	0.02473	102.41723	5.41188	0.92146	0.04433	4953.63	42.99	4710.13	53.14	4210.06	148.71	559	165
D-1-13	0.48692	0.01815	13.30536	0.68336	0.19886	0.00784	4202.08	55.07	2701.56	48.50	1169.20	42.13	602	35
D-1-14	0.65925	0.03261	34.63900	2.34831	0.38060	0.01995	4644.34	71.39	3628.41	66.91	2079.06	93.15	671	94
D-1-16	0.60240	0.02424	25.80982	1.18464	0.33011	0.01468	4513.81	58.46	3339.36	44.87	1838.94	71.14	717	64
D-1-17	0.58013	0.03145	23.71232	1.42108	0.31098	0.01365	4459.00	78.98	3256.64	58.39	1745.51	67.12	726	76
D-1-18	0.50764	0.02469	14.15692	0.76965	0.21527	0.00993	4263.54	71.61	2760.28	51.56	1256.85	52.68	619	47
D-1-19	0.78729	0.02575	63.48637	3.25911	0.58664	0.02519	4898.91	46.63	4230.55	51.32	2975.80	102.35	490	110
D-1-20	0.55094	0.03077	20.04379	0.86797	0.28115	0.01090	4383.66	81.67	3093.47	41.88	1597.15	54.85	716	67
D-1-21	0.59621	0.02914	25.13859	1.58716	0.31361	0.01450	4498.78	71.04	3313.61	61.66	1758.45	71.17	696	72
D-1-23	0.31827	0.02228	6.51448	0.37749	0.15619	0.00563	3561.50	107.71	2047.86	51.01	935.55	31.37	664	34
D-1-22	0.50581	0.02334	15.86042	0.90903	0.23966	0.00969	4258.23	67.94	2868.43	54.74	1384.93	50.41	690	48
D-1-24	0.53582	0.02136	15.09406	0.76710	0.20619	0.00789	4342.90	58.43	2821.19	48.40	1208.47	42.17	552	38
D-1-25	0.40400	0.01601	8.50137	0.34666	0.15424	0.00351	3924.04	59.53	2286.07	37.05	924.70	19.60	562	22
D-1-26	0.37966	0.01205	8.05161	0.31504	0.15294	0.00372	3830.40	47.95	2236.83	35.34	917.44	20.77	584	19
D-1-27	0.51094	0.02130	15.62586	0.77745	0.23295	0.00829	4273.08	61.34	2854.20	47.48	1349.94	43.35	663	42

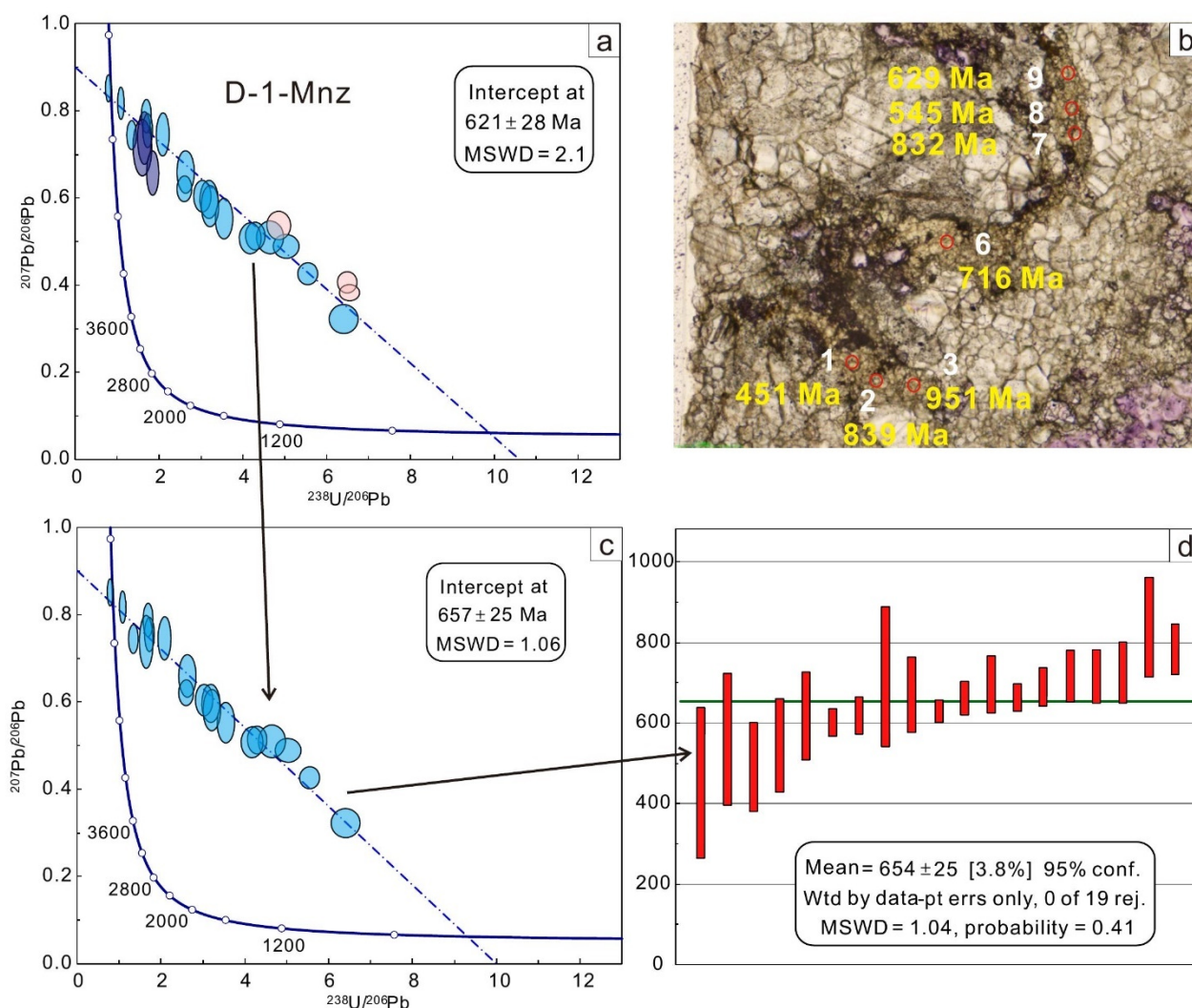


**Figure 8.** Monazite Concordia diagram of sample D-1 from the Bayan Obo deposit. (a) The Intercept age of all dates. (b) The detail testing locations and age distribution characteristics in monazite. (c) The Intercept age of the blue group. (d) The mean age dates of the blue group.

The monazite in sample Fe-1 presents coarse-grained crystals up to  $\sim 600 \mu\text{m}$  in size. The corrected intercept of the  $^{207}\text{Pb}$  age was divided into three groups. The dominant age group yielded a weighted  $^{206}\text{Pb}$  mean age of  $763 \pm 16$  Ma ( $\text{MSWD} = 1.3$ ). The maximum and minimum single-point ages were  $1393 \pm 142$  Ma and  $429 \pm 24$  Ma, respectively. The ages of single monazites also vary widely (Table 2 and Figure 9).

**Table 2.** Monazite U–Pb isotopic data of the sample Fe-1 from the Bayan Obo deposit.

Sample	$^{207}\text{Pb}/^{206}\text{Pb}$		$^{207}\text{Pb}/^{235}\text{U}$		$^{206}\text{Pb}/^{238}\text{U}$		$^{207}\text{Pb}/^{206}\text{Pb}$		$^{207}\text{Pb}/^{235}\text{U}$		$^{206}\text{Pb}/^{238}\text{U}$		Corrected $^{207}\text{Pb}$	
	Ratios	Error	Ratios	Error	Ratios	Error	Age (Ma)	Error	Age (Ma)	Error	Age (Ma)	Error	Age (Ma)	Error
Fe-1-1	0.59700	0.01559	18.74333	0.72809	0.22913	0.00676	4880.51	76.61	3943.49	48.83	2475.79	106.60	586	29
Fe-1-2	0.40577	0.01559	8.48333	0.40837	0.15323	0.00519	4582.06	28.50	3472.41	30.81	1892.17	42.55	588	25
Fe-1-3	0.40662	0.02077	6.03316	0.35152	0.11113	0.00502	2847.19	92.28	1604.87	40.55	859.92	18.20	429	24
Fe-1-4	0.77989	0.01791	59.06623	1.93758	0.55223	0.01495	2975.90	112.06	1707.59	63.84	902.13	34.29	731	67
Fe-1-5	0.48992	0.02331	15.76650	0.95309	0.23670	0.00986	2676.37	115.06	1509.43	52.77	864.71	25.56	769	47
Fe-1-6	0.49203	0.03850	12.23397	1.14521	0.18235	0.00946	4050.90	205.25	2639.43	95.46	1344.44	116.95	594	55
Fe-1-7	0.69309	0.01506	35.64064	1.33451	0.37022	0.01098	3495.06	142.21	2239.48	90.34	1159.05	40.22	705	41
Fe-1-8	0.80495	0.04617	50.20192	3.05863	0.47543	0.02700	3888.22	633.11	3043.27	107.94	1965.76	176.23	555	147
Fe-1-9	0.35359	0.02748	8.25545	0.57974	0.17825	0.00769	3745.91	136.90	2782.65	99.43	1889.16	151.40	741	44
Fe-1-10	0.65054	0.05886	34.63041	2.58078	0.44640	0.02957	3890.56	80.23	1936.34	49.12	664.61	28.96	965	177
Fe-1-11	0.44474	0.02639	11.41670	0.45671	0.20529	0.00860	4865.96	33.47	4106.13	30.08	2752.26	58.88	730	46
Fe-1-12	0.71436	0.01135	38.40415	1.66262	0.38593	0.01433	4713.07	37.20	3436.33	23.49	1721.49	35.74	681	37
Fe-1-13	0.65107	0.01360	32.84459	1.10410	0.36743	0.01083	4751.79	22.66	3675.41	40.81	2014.93	61.17	799	39
Fe-1-14	0.62896	0.01244	31.08316	1.00418	0.36036	0.01017	4441.26	49.50	2835.57	34.27	1174.62	33.34	835	37
Fe-1-15	0.51912	0.01689	17.34889	0.44353	0.25025	0.00712	4722.35	30.93	3618.00	36.54	1957.39	48.45	764	34
Fe-1-16	0.20001	0.01198	3.92425	0.20944	0.14787	0.00396	4444.17	41.06	2926.70	34.43	1260.27	36.90	765	23
Fe-1-17	0.57160	0.02012	15.82556	0.59317	0.20697	0.00670	3926.30	55.47	2315.83	53.59	942.40	34.36	565	32
Fe-1-18	0.41006	0.01696	10.68892	0.49094	0.19242	0.00599	4603.25	42.27	3432.70	28.28	1816.76	48.61	728	30
Fe-1-19	0.27562	0.01783	5.60242	0.32951	0.15946	0.00599	4243.14	115.93	2723.22	91.67	1235.53	86.27	746	33
Fe-1-20	0.29961	0.01603	6.88224	0.40906	0.17086	0.00634	4322.74	47.07	2932.21	24.50	1388.81	34.84	771	33
Fe-1-21	0.18286	0.01271	3.53845	0.24038	0.14822	0.00493	4086.85	88.06	2526.31	36.93	1152.77	43.10	783	28
Fe-1-22	0.49235	0.01494	15.47645	0.45993	0.23642	0.00605	4017.99	50.82	2539.35	34.83	1128.95	27.86	764	30
Fe-1-23	0.22036	0.01533	4.49083	0.35139	0.15343	0.00651	4216.31	44.79	2815.43	26.63	1331.92	28.26	773	35
Fe-1-24	0.29517	0.03028	6.18301	0.55655	0.16453	0.00790	4196.54	70.09	2836.48	55.81	1347.57	48.68	748	47
Fe-1-25	0.68815	0.01699	29.14441	0.67347	0.31413	0.00713	4646.85	120.71	3623.78	75.67	2304.34	127.46	611	37
Fe-1-26	0.32395	0.02281	8.70527	0.72037	0.20659	0.00999	3340.86	101.19	1885.52	49.64	920.77	30.77	894	51
Fe-1-27	0.35937	0.03238	14.76847	1.55106	0.34666	0.03219	3690.20	113.48	2224.68	60.98	1042.41	41.97	1393	143
Fe-1-28	0.29364	0.20272	22.49282	2.60820	0.39374	0.03509	3430.82	159.33	1975.98	76.24	962.93	38.93	1737	523
Fe-1-30	0.21166	0.01217	4.02332	0.23191	0.14694	0.00468	2917.10	93.06	1629.72	46.42	875.09	25.37	749	26

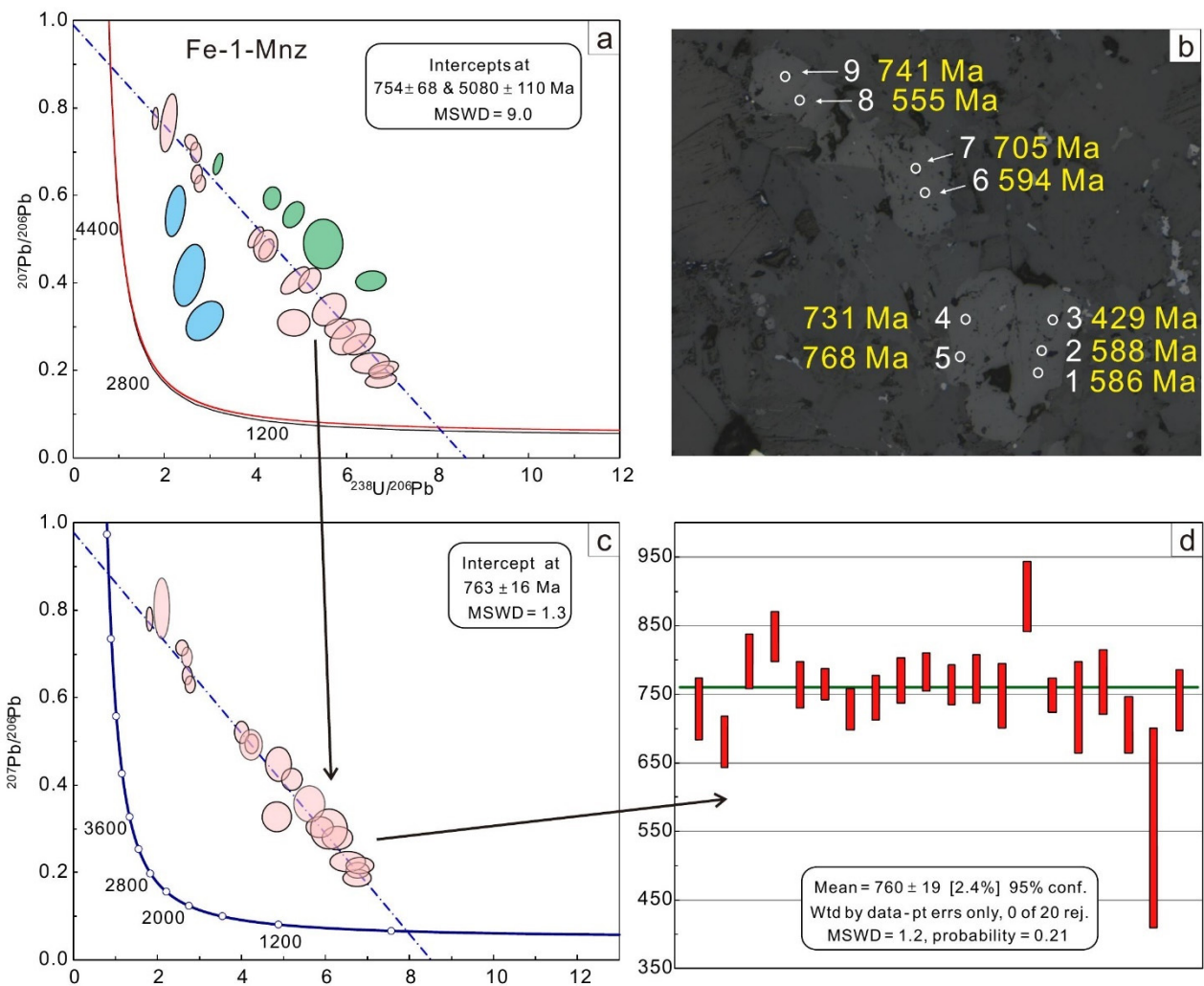


**Figure 9.** Monazite Concordia diagram of sample Fe-1 from the Bayan Obo deposit. (a) The Intercept age of all dates. (b) The detail testing locations and age distribution characteristics in monazite. (c) The Intercept age of the pink group. (d) The mean age dates of the pink group.

The monazite in sample B-2 has coarse-grained crystals with sizes up to 300  $\mu\text{m}$ . U–Pb dating of the coarse-grained crystal site yielded an intercept  $^{207}\text{Pb}$  age of  $689 \pm 22$  Ma ( $\text{MSWD} = 8.1$ ). The ages (22 dates) can also be divided into two groups:  $651 \pm 15$  Ma ( $\text{MSWD} = 2.5$ ) and  $723 \pm 14$  Ma ( $\text{MSWD} = 2.2$ ). Some monazite grains show old cores and new rims. The maximum and minimum ages of a single point were  $818 \pm 31$  Ma and  $597 \pm 15$  Ma, respectively (Table 3 and Figure 10).

**Table 3.** Monazite U–Pb isotopic data of the sample B-2 from the Bayan Obo deposit.

Sample	$^{207}\text{Pb}/^{206}\text{Pb}$		$^{207}\text{Pb}/^{235}\text{U}$		$^{206}\text{Pb}/^{238}\text{U}$		$^{207}\text{Pb}/^{206}\text{Pb}$		$^{207}\text{Pb}/^{235}\text{U}$		$^{206}\text{Pb}/^{238}\text{U}$		Corrected $^{207}\text{Pb}$	
	Ratios	Error	Ratios	Error	Ratios	Error	Age (Ma)	Error	Age (Ma)	Error	Age (Ma)	Error	Age (Ma)	Error
B-2-2	0.76534	0.04117	89.58931	5.63648	0.90126	0.06512	4858.56	76.84	4575.66	63.18	4141.93	220.80	769	273
B-2-3	0.24663	0.01246	4.62578	0.27175	0.13669	0.00398	3163.26	80.14	1753.93	49.05	825.92	22.58	648	22
B-2-4	0.25808	0.01587	4.96290	0.38695	0.13823	0.00495	3235.04	96.94	1813.02	65.89	834.66	28.01	644	27
B-2-5	0.13698	0.00444	2.26374	0.07494	0.12077	0.00172	2189.41	56.37	1201.07	23.31	735.01	9.88	671	10
B-2-6	0.10245	0.00497	1.59006	0.08393	0.11236	0.00191	1669.02	89.70	966.32	32.90	686.46	11.07	654	12
B-2-7	0.16856	0.00625	2.87617	0.11949	0.12360	0.00177	2543.41	62.16	1375.69	31.30	751.26	10.16	658	11
B-2-8	0.43299	0.00937	11.89832	0.36891	0.19774	0.00381	4027.80	32.30	2596.43	29.04	1163.18	20.51	661	18
B-2-9	0.10831	0.00421	1.74606	0.07714	0.11747	0.00233	1771.20	71.00	1025.71	28.53	715.97	13.46	678	14
B-2-10	0.11188	0.00687	1.61725	0.11641	0.10354	0.00244	1830.10	111.29	976.92	45.16	635.13	14.22	597	15
B-2-11	0.25206	0.00997	5.56964	0.27917	0.15492	0.00289	3197.75	62.59	1911.42	43.15	928.47	16.14	726	17
B-2-12	0.13511	0.00528	2.39408	0.09745	0.12886	0.00207	2165.47	68.09	1240.83	29.15	781.35	11.84	716	12
B-2-13	0.07791	0.00383	1.29121	0.05956	0.12162	0.00163	1144.46	97.74	841.83	26.39	739.87	9.38	728	10
B-2-14	0.26798	0.00843	5.86563	0.23032	0.15777	0.00285	3294.26	49.39	1956.16	34.06	944.36	15.90	720	16
B-2-15	0.09276	0.00319	1.56069	0.05965	0.12222	0.00252	1483.06	65.08	954.74	23.65	743.30	14.49	718	15
B-2-16	0.20569	0.00630	4.13203	0.15643	0.14509	0.00211	2871.92	49.81	1660.66	30.95	873.39	11.90	730	12
B-2-17	0.47021	0.01679	12.98280	0.76921	0.19941	0.00822	4150.42	52.89	2678.41	55.86	1172.16	44.20	613	35
B-2-18	0.13306	0.00684	2.03875	0.11279	0.11060	0.00222	2138.71	89.83	1128.54	37.69	676.23	12.89	619	13
B-2-19	0.32755	0.02100	7.92754	0.68923	0.16800	0.00839	3605.67	98.35	2222.82	78.39	1001.10	46.33	693	42
B-2-20	0.33448	0.01423	9.79665	0.54656	0.20182	0.00577	3637.75	65.12	2415.84	51.40	1185.08	30.96	818	31
B-2-21	0.08284	0.00323	1.38301	0.05593	0.12151	0.00162	1265.55	76.03	881.72	23.83	739.23	9.32	723	10
B-2-22	0.08839	0.00562	1.36849	0.08501	0.11326	0.00314	1391.03	122.09	875.52	36.45	691.67	18.18	670	19
B-2-23	0.55380	0.01299	25.19045	1.21740	0.31644	0.01130	4391.23	34.29	3315.63	47.20	1772.30	55.36	769	40
B-2-24	0.16031	0.00581	2.73478	0.13512	0.12173	0.00230	2458.90	61.22	1337.96	36.74	740.53	13.19	655	13
B-2-25	0.33153	0.01292	8.41392	0.36509	0.18920	0.00651	3624.18	59.69	2276.68	39.38	1117.06	35.28	773	31

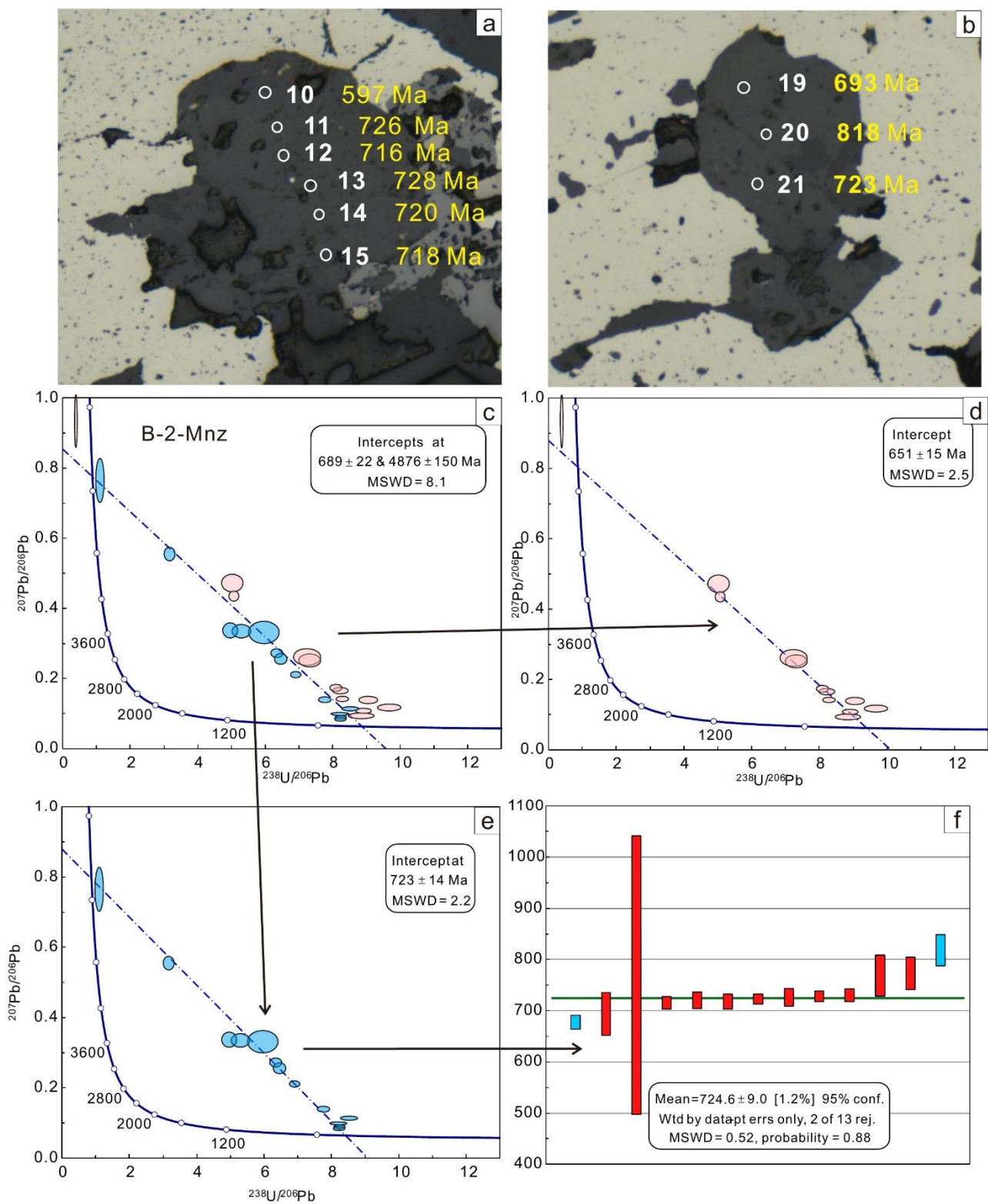


**Figure 10.** Monazite Concordia diagram of sample B-2 from the Bayan Obo deposit. (a,b) The detail testing locations and age distribution characteristics in monazite. (c) The Intercept age of all dates. (d) The Intercept age of the pink group. (e) The Intercept age of the blue group. (f) The mean age dates of the blue group.

## 6. Discussion

Before analyzing the age of the Bayan Obo deposit, the ages of basements and dikes around the deposit need to be discussed in detail.

### 6.1. Basement Ages

The basement in the Bayan Obo area comprises the Archean Wutai Group and the Proterozoic Bayan Obo Group. The U–Pb zircon ages of the basement occupy the time intervals of 2.6–2.5 Ga and 2.1–1.8 Ga, with Pb–Pb ages at ~1.5 Ga, Th–Pb ages at ~1.1 Ga, and Rb–Sr ages at ~985 Ma [34–36] (Figure 11). The order of the age distributions is U–Pb > Pb–Pb > Th–Pb > Rb–Sr. This distribution clearly reflects the closure temperature order of the corresponding chronological systems. It also suggests that Pb diffusion in the U–Th–Pb system occurs in the zircon of the basement rocks.

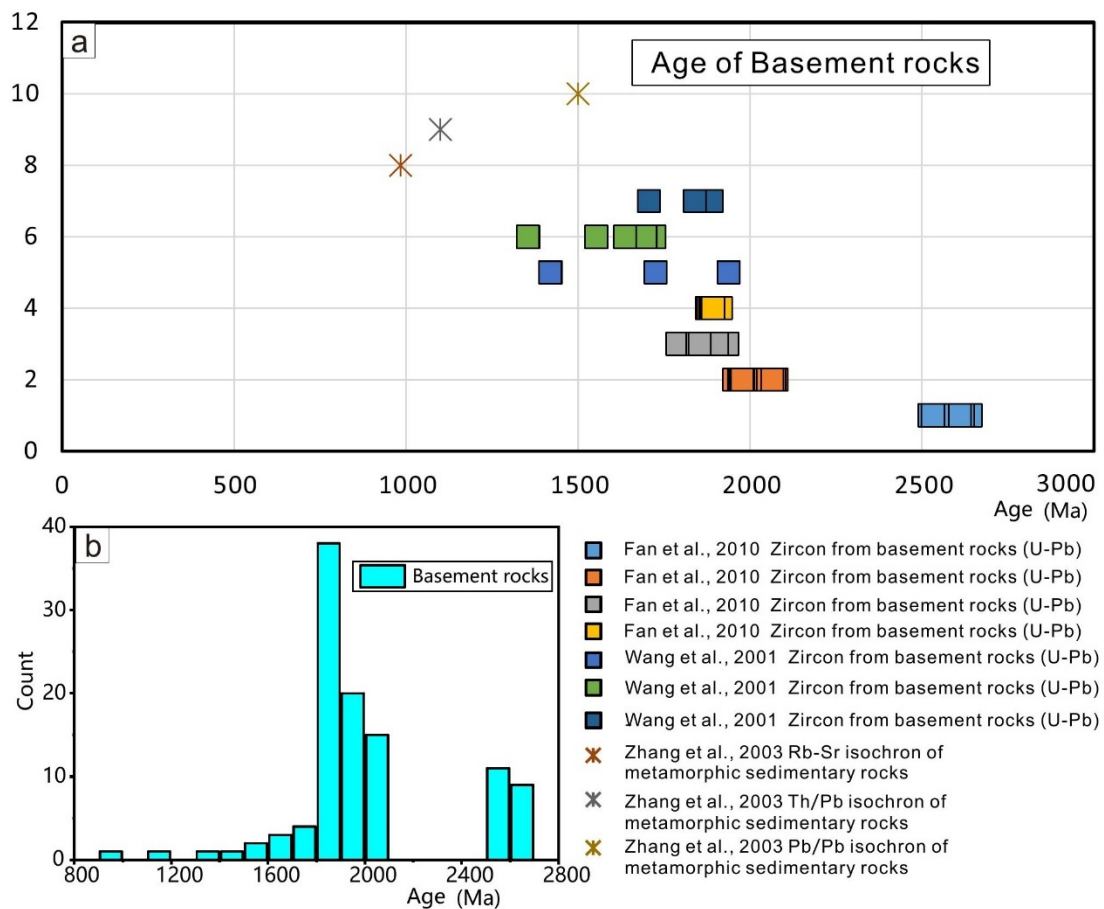


**Figure 11.** Age distribution characteristics of basement rocks. (a) Single age distribution characteristics corresponding to different studies. (b) Stack histograms of all ages [34–36].

The basement rocks at Bayan Obo are part of the NCC and are composed of Neoproterozoic mylonitic granite gneiss ( $2588 \pm 15$  Ma), Paleoproterozoic syenite and granodiorite ( $2018 \pm 15$  Ma), and biotite granite gneiss and garnet-bearing granite gneiss (~1890 Ma) [35]. The peak ages of ~2.5 Ga and ~1.9 Ga reflect two crustal growth events with prominent magmatism in the mobile belt around the NCC.

### 6.2. Dike Ages

The rocks around the dike consist mainly of carbonate, fenite, and quartz conglomerates. The age summary of previous works along our current study is shown in Figure 12 [1,3,37–42]. The main ages are concentrated at ~2.6–2.4 Ga, ~2.1–1.8 Ga, and

~1.5–1.0 Ga. The ~1.5–1.0 Ga age range represents the Th–Pb age of apatite, and the apatite Th–Pb closure temperature is lower than that of zircon U–Pb, reflecting the closure system. The zircon U–Pb dates in Liu et al. [37] are more widely scattered and younger than other zircon single-grain U–Pb dates from the Wu dike to ~200 Ma. This is unreasonable to some extent: if a zircon age of ~200 Ma was produced in this period, it would mean that the area or a very small part of it reached at least ~840 °C. Since the Wu dike is a very small area, it would have reset most of the older zircon ages, and the apatite Th–Pb ages would have certainly been reset as well. This is clearly inconsistent with the geological data, so the geological significance of this age should be considered carefully. Alternatively, the ~200 Ma difference could reflect localized fluid alteration or deformation with no need for dramatically different temperature. Ni et al [43] consider the Caledonian age of  $368 \pm 43$  Ma from the Rb–Sr dating of fluid inclusions in quartzite around the Wu dike may correspond to the timing of carbonatitic fluid activity; the fluid activity is caused by the intrusion of the carbonatite dike. Maybe the dikes around Bayan Obo need some new entry points to reach a summary of opinions.

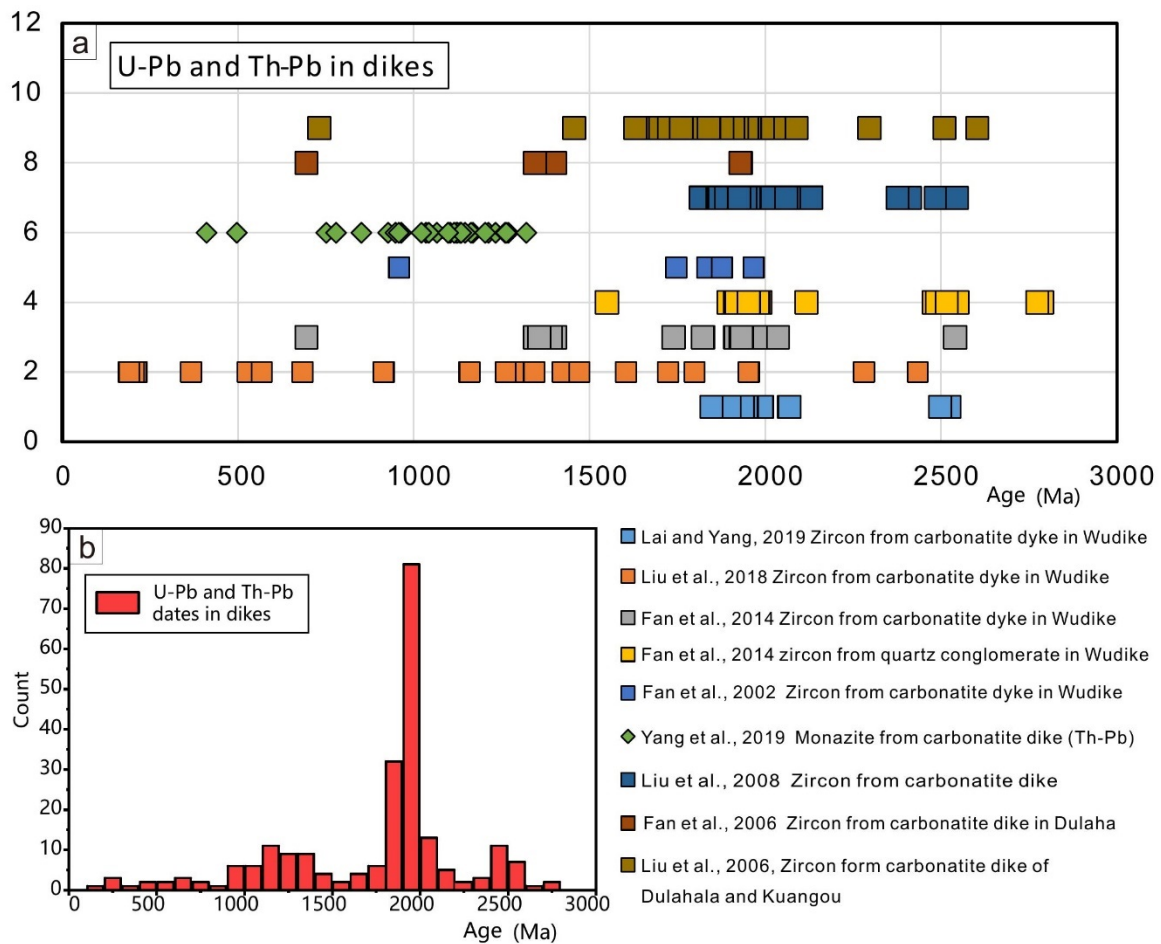


**Figure 12.** Age distribution characteristics of U–Pb and Th–Pb in carbonatite. (a) Single age distribution characteristics corresponding to different studies. (b) Stack histograms of all ages [1,3,37–42].

### 6.3. Carbonatite Ages

In previous studies, carbonatite samples from the Bayan Obo area were mainly collected from dike areas and dated using whole-rock Sm–Nd analysis [1,3,34,42,44]. The Sm–Nd age is ~1.3 Ga (Figure 13), and the whole-rock Sm–Nd system has not been reset within the Bayan Obo area [5]. Another advantage of Sm–Nd analysis over zircon U–Pb analysis is that it avoids the influence caused by the mixing of the ages from the basement zircons. According to the Sm–Nd system, the Wu, Jianshan, and Dulahala carbonate dikes

formed at ~1.3 Ga. Sm and Nd are REE. The monazite of Th–Pb dates in the carbonatite dike ranged from  $411 \pm 6$  Ma to  $1321 \pm 14$  Ma in age [1]. The in situ Nd isotopic measurements of monazite from the carbonatite dike yielded an isochron age of  $1275 \pm 87$  Ma [3]. Thus, the monazite in the dike has the same initial age, i.e., ~1.3 Ma.

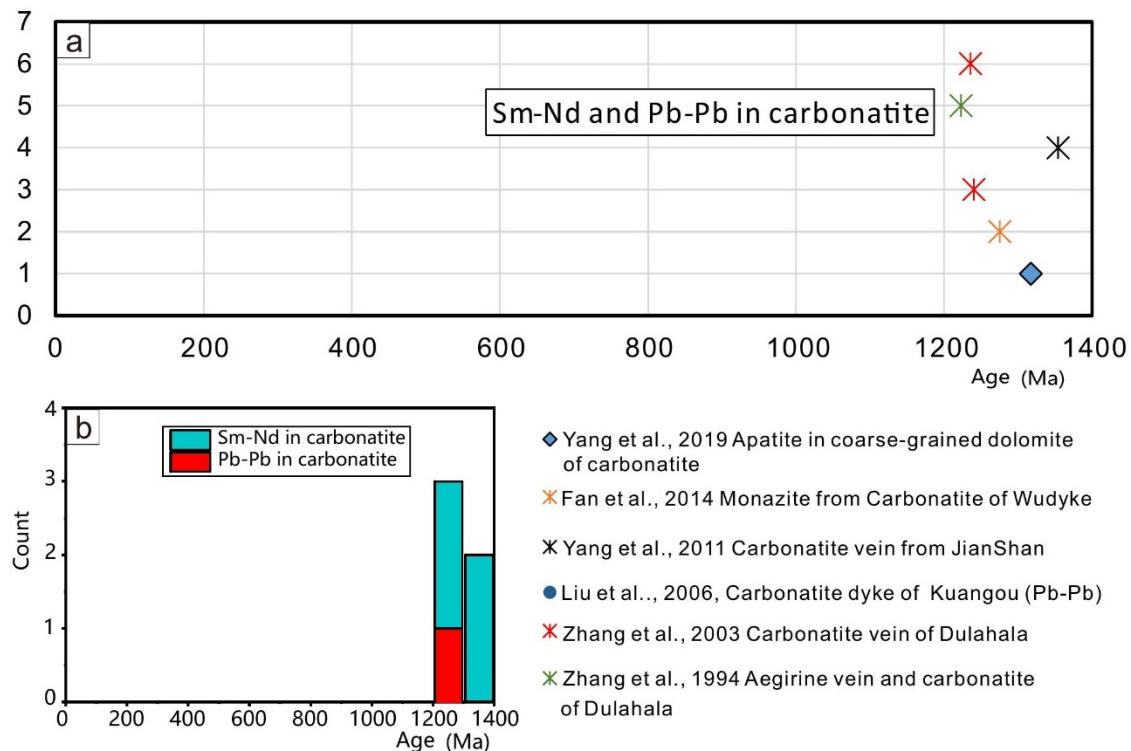


**Figure 13.** Age distribution characteristics of Sm–Nd and Pb–Pb in slate. (a) Single age distribution characteristics corresponding to different studies. (b) Stack histograms of all ages [1,3,34,42,44].

The U–Pb zircon ages of carbonatite showed mean  $^{207}\text{Pb}/^{206}\text{Pb}$  ages of  $2521 \pm 25$  Ma and  $1921 \pm 14$  Ma [39]. Fan et al. [3] reported a SHRIMP U–Pb in three zircon crystals from the carbonatite, which have a weighted mean  $^{207}\text{Pb}/^{206}\text{Pb}$  age of  $1418 \pm 29$  Ma, and an isotopic dilution (ID-TIMS) age of zircon from the same carbonatite dike is  $1416 \pm 77$  Ma. The ages of the two papers are very different, and the ages of the carbonatite by Fan et al. [3] were ~2.5 Ga and ~1.9 Ga. This means that the carbonatite contains zircon sourced from the basement rocks, which also explains the age span in the dike in Figure 12.

#### 6.4. Granite Ages

Granitoids are extensively spread near the Bayan Obo deposit and have Permian–Triassic ages, for example: 246–270 Ma (K–Ar, [24]),  $264 \pm 91$  Ma or  $249 \pm 35$  Ma (Rb–Sr isochron, [34]),  $255.2 \pm 8.2$  Ma (Rb–Sr isochron, [45]), 243–293 Ma (zircon U–Pb, [25,46,47]), and ~180 Ma and ~99 Ma (apatite fission track age, [4]; Figure 14).

According to the *T–T* model of Tian et al. [4], the granite experienced a rapid cooling process between ~300 and ~54 Ma (especially ~300–180 Ma), reflecting rapid uplift and exhumation. This process resulted in widespread fracturing of the slate east of the Bayan Obo deposit.

All granitoids formed in a post-collisional tectonic regime at a convergent margin, consistent with plate subduction during the closure of the Paleo-Asian Ocean (PAO), which began in the Neoproterozoic and continued until the Carboniferous–Permian [25].

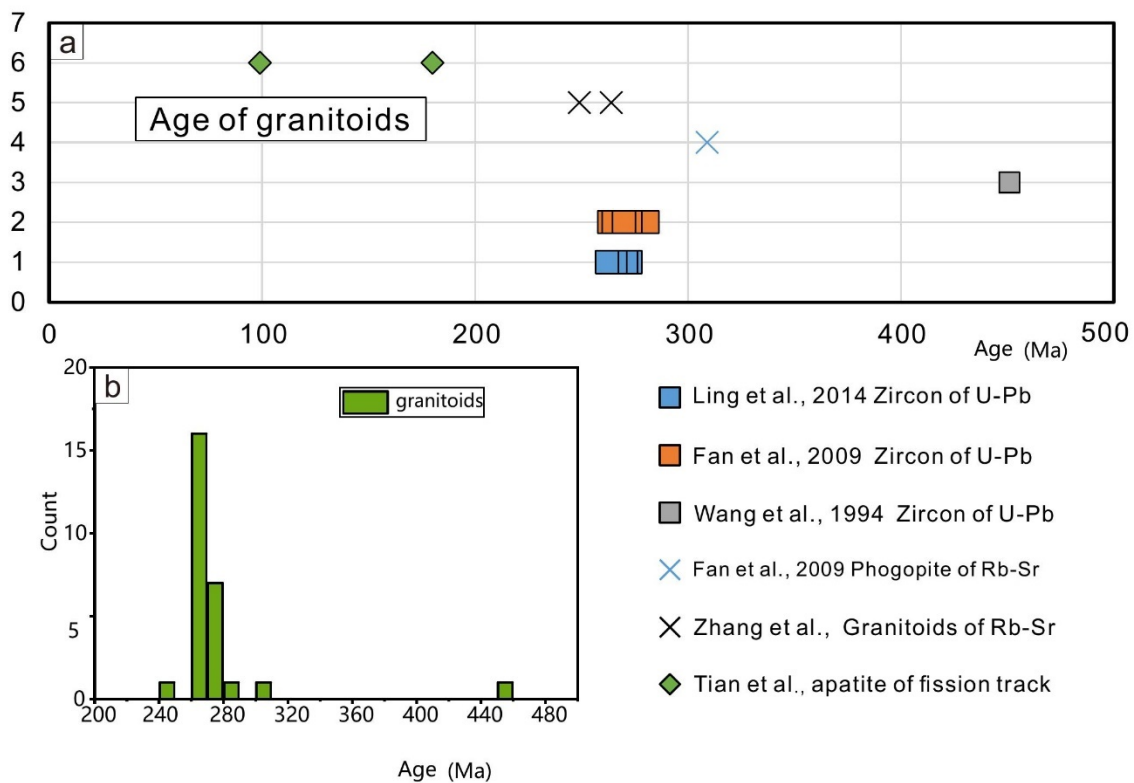


**Figure 14.** Age distribution characteristics of the granitoids. (a) Single age distribution characteristics corresponding to different studies. (b) Stack histograms of all ages [4,24,25,34,45–47].

### 6.5. Slate Ages

Slate in the Bayan Obo mining area is covered on the H8 formation and has a wide age span [21,34,48]. The ages can be divided into five main stages: ~2.5, ~1.3, ~1.0, ~0.4–0.5, and ~0.2 Ga (Figure 15). From Figure 15, we can deduce that the Rb–Sr system was completely reset during ~0.4–0.5 Ga, while the Sm–Nd system was almost unaffected. SIMS U–Pb and LA-ICP-MS Th–Pb zircon dating results demonstrate that the formation of igneous rocks in the H9 member is around 1.4 Ga (represented by the zircons with the oldest  $^{208}\text{Pb}/^{232}\text{Th}$  age of 1.41 Ga), which is older than the age of the ore-bearing dolomite (~1.3 Ga) [9].

The ~2.5 Ga zircon grains in the slate have the same age as the basement, so they are inherited from the basement rocks. The ~1.3 Ga data contain zircon U–Pb and whole-rock Sm–Nd ages, indicating the timing of the first metallogenic hydrothermal fluid that penetrated H8 into H9.

In the PAO, the major volcanic arc and marginal basin formation events occurred at 1000–1010, 830, 740–700, and 670 Ma [49]. The ~1.0 Ga age event of the slate in the Bayan Obo area is consistent with volcanic arc and marginal basin formation during the first phase of the PAO. The ~0.4–0.5 Ga age of the slate is consistent with the tectonic movement of the Caledonian age, and the dynamic background is the last volcanic arc and marginal basin formation event in the PAO. Whether mineralization occurred during this time requires further analysis of the ore age in the mine area. The ~0.2 Ga age is consistent with granite intrusion in the periphery of the mine area.

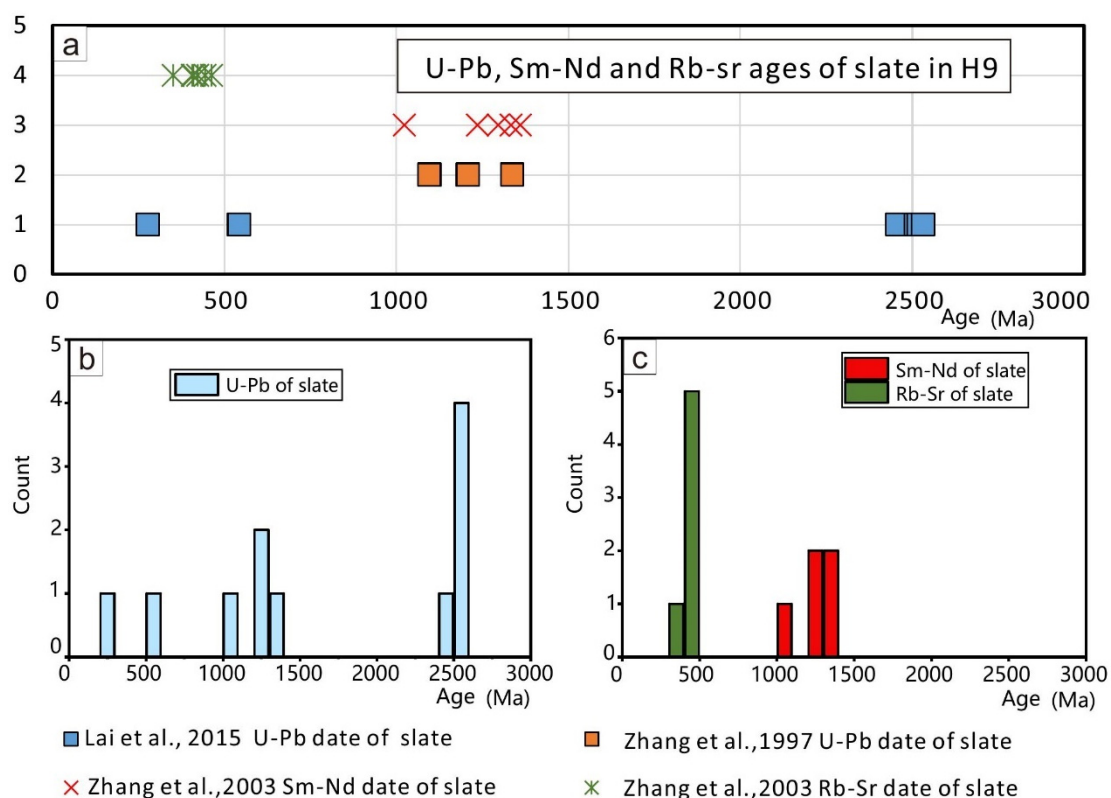


**Figure 15.** Age distribution characteristics of U–Pb and Th–Pb of slate from H9. (a) Single age distribution characteristics corresponding to different studies. (b,c) Stack histograms of all ages [9,21,34,48].

### 6.6. Ore Body Ages

The ore body of the Bayan Obo deposit has much age data, encompassing all common dating techniques except U–Th–Pb dating of fluorite, dolomite, and calcite. Combining the basement, dike, granite, and ore ages, the Bayan Obo Fe–REE–Nb deposit experienced four main thermal events:  $\sim 1.3$ ,  $\sim 1.0$ ,  $\sim 0.8$ , and  $\sim 0.4$  Ga.

#### 6.6.1. Re–Os, Rb–Sr, and Ar–Ar Ages

The approximate age distribution of the Re–Os, Rb–Sr, and Ar–Ar dating methods is shown in Figure 16 [21,34,50–54], which is consistent with recorded closure temperature ranges [15]. The ages of all three methods indicate large-scale and continuous thermal activity during  $\sim 0.4$  Ga, and a hydrothermal fluid temperature as low as  $350$  °C. In Zhang et al. [34], the Rb–Sr age of hematite ore and country rocks of the Middle North Mine is  $1166 \pm 41$  Ma. The North Mine has different provenance characteristics (e.g., different Sr isotopic composition) than the Main and East Mines, and may have formed in a continental basin environment.

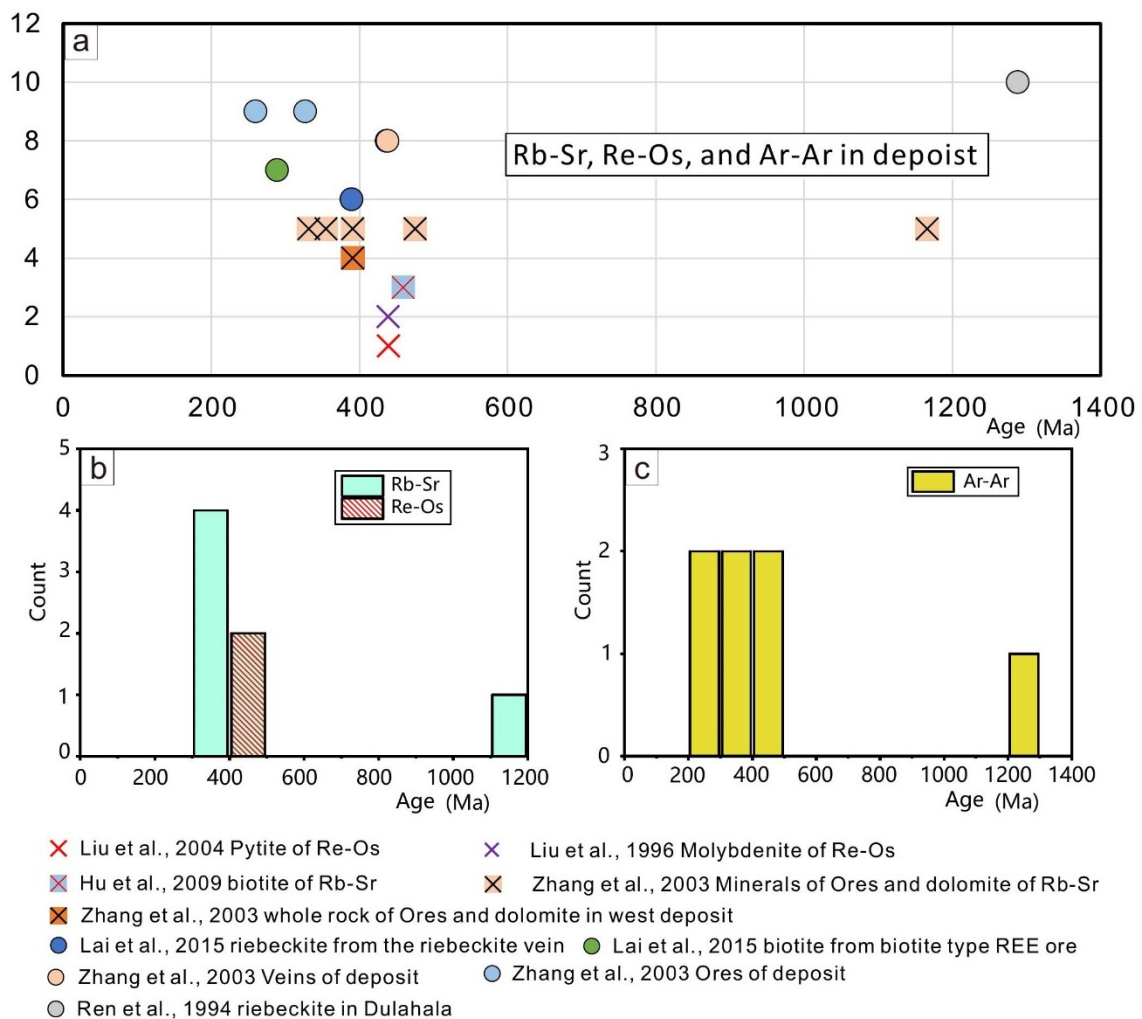


**Figure 16.** Age distribution characteristics of Rb–Sr, Re–Os, and Ar–Ar in the ore deposit. (a) Single age distribution characteristics corresponding to different studies. (b,c) Stack histograms of all ages [21,34,50–54].

### 6.6.2. Th–Pb Ages

The Th–Pb ages are mainly from monazite, bastnaesite, zircon, and the whole rock [6–8,17,34,46,54–58]. Zircon U–Th–Pb dating is scarce within the Bayan Obo deposit, mainly because the orebody lacks zircons. Only Campbell et al. [57], Zhang et al. [58], and Liu et al. [37] have reported on zircons from the ore body, all of which used Th–Pb dating. Campbell et al. [57] described the mineral assemblage in their main sample as being dominated by apatite, REE fluorocarbonates, and aegirine, which gives it a green–brown appearance, and the Th–Pb zircon core and edge ages were  $1325 \pm 60$  Ma and  $455.6 \pm 28.27$  Ma, respectively. Zhang et al. [58] noticed that zircons from the carbonatite sills of the Bayan Obo ore deposit have a uniform  $^{208}\text{Pb}/^{232}\text{Th}$  age with a weighted average of  $1301 \pm 12$  Ma. Liu et al. [37] reported that dolomite samples have many zircons, providing no supporting images or detailed description of the rock itself.

According to previous studies, part of the Bayan Obo deposit experienced a high-temperature thermal event after  $\sim 1.3$  Ga, and the monazite and bastnaesite may have fused into zircon; this maybe represents the partial recrystallization of monazite, bastnaesite, and zircon. The zircon closure temperature of the U–Th system is higher than that of Th–Pb [16]. There is likely fluid-aided trace element diffusion at relative lower temperatures. Therefore, we suggest that the Th–Pb age of zircon is the only proof that the system had

hydrothermal activity at a certain temperature at this time; however, it is not proof that REE mineralization started.

The whole-rock  $^{238}\text{U}/^{204}\text{Pb}$  and  $^{232}\text{Th}/^{204}\text{Pb}$  isochron diagrams for Nb–REE–Fe ores, Nb–REE ores, and dolomites from the western Bayan Obo deposit are  $557 \pm 280$  Ma and  $438 \pm 67$  Ma, respectively [34]. The monazite U–Pb closure temperature range is 840–780 °C, and its Th–Pb confinement temperature range is slightly lower than that of U–Pb; therefore, the age of  $557 \pm 280$  Ma records the beginning of a high-temperature thermal event, but the error is large, and this high-temperature thermal event may have started later or earlier (Figure 17).

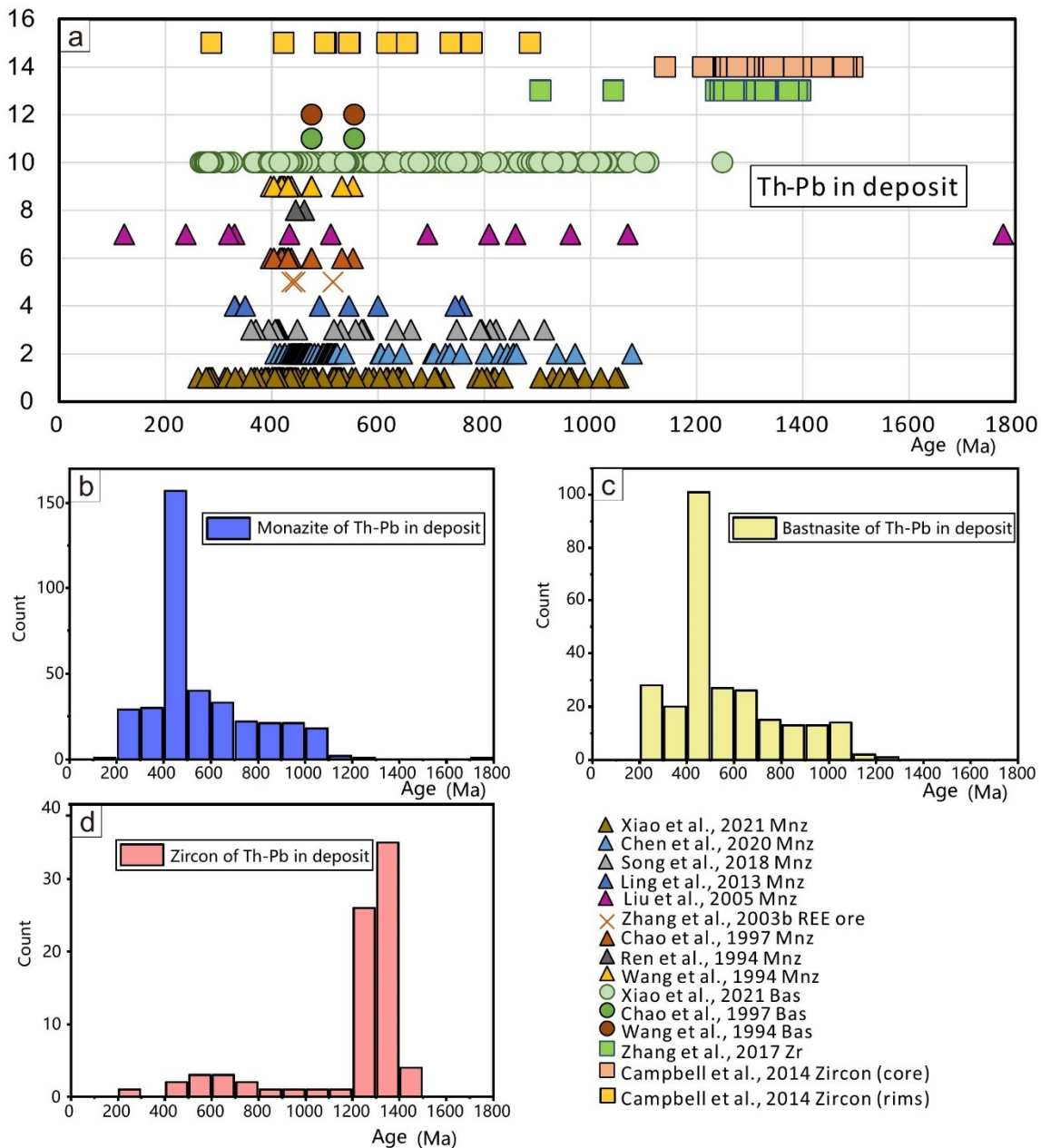


**Figure 17.** Age distribution characteristics of Th–Pb in the ore deposit. (a) Single age distribution characteristics corresponding to different studies. (b–d) Stack histograms of all ages [6–8,17,34,46,54–58].

The range and peak Th–Pb age distribution of monazite and bastnaesite in the ore body are basically the same, with peak values of ~0.4–0.5 Ga and ranges of ~0.2–1.3 Ga, suggesting that their formation periods are consistent. From the slate ages, a high-temperature

fluid crossed H8 into H9 during  $\sim 0.4\text{--}0.5$  Ga. This fluid modified the rock within H8 by increasing the temperature. One possible explanation for the spike in the  $\sim 0.4\text{--}0.5$  Ga Th–Pb ages of monazite and bastnaesite is that the REE hydrothermal fluid has relatively balanced amounts of Th and Pb, compensating for the loss of Th and Pb during  $\sim 1.3\text{--}0.5$  Ga. According to Song et al. [6], the structural relationships and extreme isotopic variability of the Bayan Obo monazite suggest that it is the product of dissolution and precipitation and that its Th–Pb budget has been altered over an extended period. Thus, another possible explanation for the peak age  $\sim 0.4\text{--}0.5$  Ga age is the resetting of the Th–Pb isotopic system due to high temperature and hydrothermal alteration. This point is supported by an intense Caledonian tectonic-thermal event of the Bayan Obo deposit [25,52], and the Th–Pb ages of monazite from dikes that are mainly concentrated at  $\sim 1.1\text{--}1.3$  Ga and have an initial age of  $1321 \pm 14$  Ma [1].

### 6.6.3. U–Pb Ages

The whole-rock Pb–Pb isochron age of dolomite rock from the main and east mine, and the Wu dike is  $1.31 \pm 0.28$  Ga, the whole rock U–Pb age of the biotite apatite Nb–REE ore from the East Mine is  $523 \pm 23$  Ma, and the whole-rock isochron U–Pb age of the Nb–REE–Fe ore and Nb–REE ore from the West Mine is  $557 \pm 280$  Ma [34]. The  $\sim 1.3$  Ga is the same time as the dike intrusion, suggesting that the initial ore-forming and intrusive thermal events occurred during the same period.

The ages of monazites in samples D-1, Fe-1, and B-2 are different, but their overall distribution ranges are essentially the same (Figure 18). The age of the monazite in Fe-1 with the largest age range may represent the beginning and end of REE mineralization in the Bayan Obo deposit, that is, from  $1393 \pm 142$  Ma to  $429 \pm 24$  Ma.

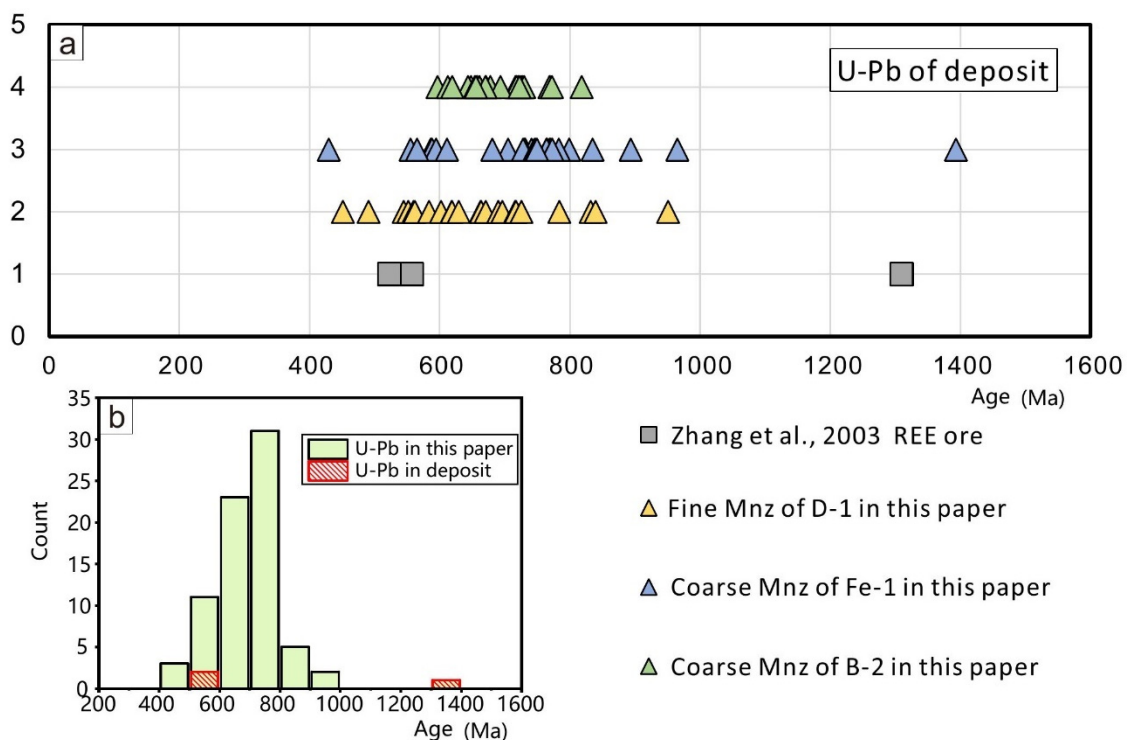


**Figure 18.** Age distribution characteristics of U–Pb in the ore deposit. (a) Single age distribution characteristics corresponding to different studies. (b) Stack histograms of all ages [34].

### 6.6.4. Sm–Nd Ages

The ore Sm–Nd ages have a peak at  $\sim 0.4\text{--}0.5$  Ga,  $\sim 0.8\text{--}0.9$  Ga,  $\sim 1\text{--}1.1$  Ga, and  $\sim 1.2\text{--}1.4$  Ga [1,17,34,50,51,59,60] (Figure 19). The isotopic ages of high-temperature systems are open, and daughter products are more likely to escape at consistently higher

temperature environments, so the age differences between samples and spots in some dating systems are the result of isotopic diffusion. Although the ore body is overprinted by late hydrothermal fluids, Sm and Nd are not very mobile during alteration [8]. Only the Sm–Nd system of the minerals are reset, which is inconsistent with the whole-rock Sm–Nd system [5]. This view is also confirmed by Liu et al. [61], who reported that the Sm–Nd system of some fluorite and bastnaesite were reset during the Paleozoic alteration triggered by the closure of the PAO.

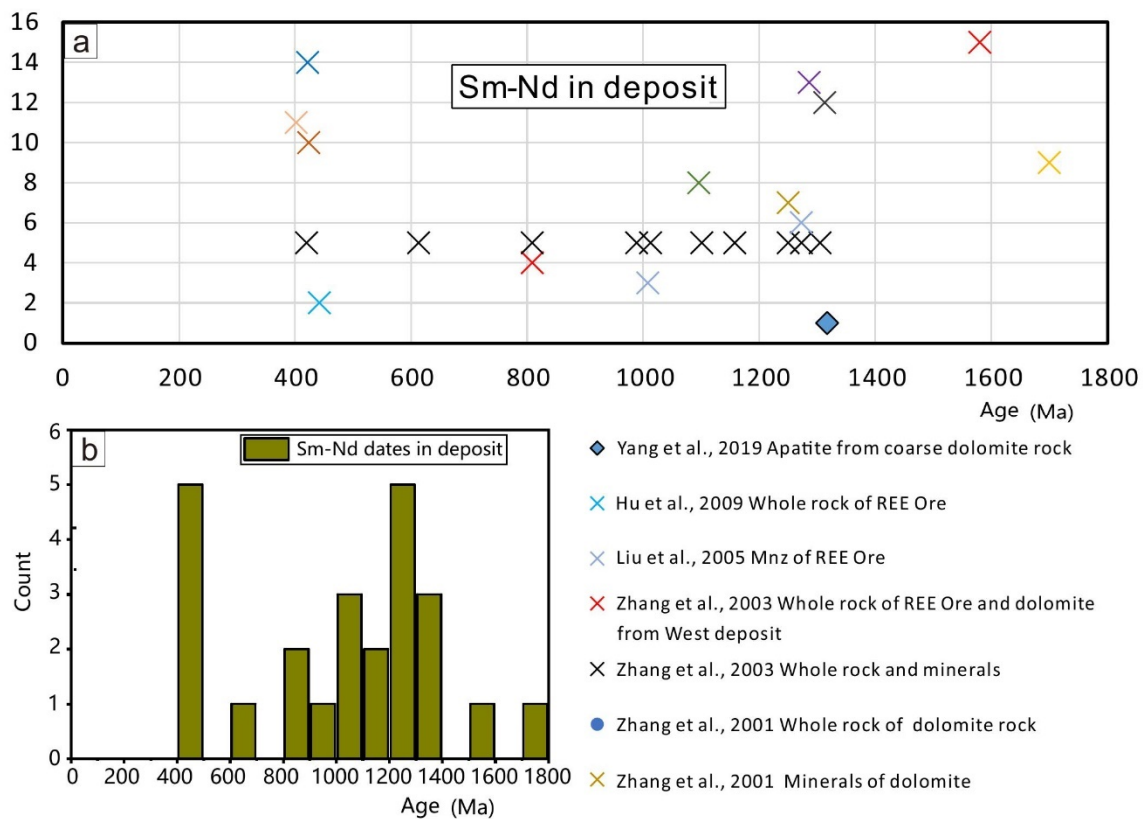


**Figure 19.** Age distribution characteristics of Sm–Nd in the ore deposit. (a) Single age distribution characteristics corresponding to different studies. (b) Stack histograms of all ages [1,17,34,50,51,59,60].

## 6.7. The Age Sequence

### 6.7.1. ~2.5 Ga

The North China Craton (NCC) is one of the best recorders of the ~2.5 Ga geological features [62]. The major tectonic-thermal events that largely occurred around ~2.5 Ga are represented by the Bayan Obo basement complex, such as the Huai'an gneiss terrane, the Dengfeng complex, and the Zunhua and Wutaishan belts. The Bayan Obo Neoproterozoic basement is mainly composed of calcalkaline tonalite–trondhjemite–granodiorite (TTG) gneiss that is dated at ~2.5 Ga [35]. The Huai'an gneiss terrane is a typical Archean terrane within the Trans-North China Orogen of the NCC and consists of the TTG suite and dioritic granulite facies gneisses that originated during a juvenile crustal formation event at 2.55–2.50 Ga by partial melting of subducted oceanic crustal material [63]. The Zunhua and Wutaishan belts (2.55–2.50 Ga) within the central orogenic belt of the NCC contain variably metamorphosed and deformed tectonic blocks of peridotite and amphibolite in a sheared metasedimentary matrix [64]. The Dengfeng complex is located at the southern margin of the NCC, and magmatic U–Pb zircon age data indicate that it is formed at the time interval of 2547–2504 Ma [65].

The ~2.5 Ga rocks can be attributed to Paleoproterozoic crustal assembly in the NCC associated with the formation of the Columbia supercontinent [66–70]. Thus, the ~2.5 Ga age documents the emplacement or formation age of the basement in the Bayan Obo area.

#### 6.7.2. ~1.9 Ga

The assembly of Columbia is completed during 2.1–1.8 Ga. Thereafter, long-lived, subduction-related accretion occurred at major continental margins from 1.8 to 1.3 Ga, and Columbia began fragmenting before ~1.6 Ga and finally broke apart by ~1.3 Ga [71,72].

After ~1.95 Ga, the Archaean to Paleoproterozoic basement of the NCC was assembled by microcontinental blocks and three Paleoproterozoic collisional belts: the Khondalite belt, the Jiao-Liao-Ji belt, and the Trans-North China Orogen [71]. At 1.85 Ga, the NCC had finally formed. During the breakup of Columbia, the Zhaertai–Bayan Obo–Huade–Weichang rift zone formed along the northern margin of the craton at 1.6–1.2 Ga [72].

Rogers and Santosh [73] indicated that the granite–granodiorite (GG) suites succeeded the older tonalite–trondhjemite–granodiorite (TTG) suites, some GG suites formed earlier, and the GG suites were disseminated in the 1.8–1.9 Ga orogenic belts. The collisional orogeny at the northern margin of the NCC between ~2.0 Ga and ~1.8 Ga brought a swarm of amphibolite–granodiorite magma and a strong regional metamorphic event [3,26]. The basement consisting of gneisses, syenite, granodiorite, and diorite experienced secondary thermal events, consistent with the onset of Zha’ertai–Bayan rifting.

The U–Pb zircon ages of TTG, carbonatite, and quartz conglomerate of the Bayan Obo area always are around ~2.5 Ga and ~1.9 Ga. Thus, the ~2.5 Ga and ~1.9 Ga events have the same geodynamic basis attributed to the assembly of the Columbia supercontinent, and the ~1.9 Ga age reflects stabilization of the craton in which subduction occurred.

#### 6.7.3. ~1.4–1.3 Ga

During 1.6–1.2 Ga, continental rifting, anorogenic magmatism, and emplacement of the mafic dike swarms were widespread across all cratonic blocks of Columbia [71,72], and the ~100 dikes of the Bayan Obo deposit were emplaced. The ~1.3 Ga age and the background of the dikes around the Bayan Obo deposit are consistent with the Yanliao large igneous province. The formation of the Yanliao large igneous province was accompanied by pre-magmatic uplift that began at 1.35–1.34 Ga ( $^{207}\text{Pb}/^{206}\text{Pb}$  ages), which was related to either a mantle plume and/or continental rifting during the breakup of the NCC from the Columbia supercontinent [44]. Together with the persistent and slow extension of the Bayan Obo rift, a low degree of partial melting occurred in the mantle lithosphere, leading to the production of carbonatite magma during the last phase of the breakup of Columbia.

The maximum corrected  $^{206}\text{Pb}$  age of the monazite of the Bayan Obo deposit in this study is  $1393 \pm 142$  Ma, which implies that initiation of REE mineralization was at ~1.4 Ga. This is consistent with the ~1.4 Ga age of the carbonatite dike [3,37,41]. Continuous evolution (crystal fractionation) resulted in abundant LREE accumulation in the terminal calcite carbonatite [44]. The period ~1.4–1.3 Ga is the major time for the formation of carbonatite dikes and REEs.

#### 6.7.4. ~1.1–0.4 Ga

After the final breakup of the NCC from the Columbia supercontinent, the northern NCC was affected by several subduction and accretion events associated with the PAO. The breakup of the large Mesoproterozoic Eurasian continent into Baltica and Siberia may have occurred no later than about 1100 Ma, and the PAO has four turning points in history at ~1000–650, ~650–510, and 510–450 Ma [49]. Major volcanic arc and marginal basin formation events in the PAO occurred at 1000–1010, 830, 740–700, 670–640, 570, 540, and 500–490 Ma, while the major phases of accretion and ridge collision occurred at about 800, 570, and 470 Ma [49]. A multistage tectonic-thermal event is consistent with the various ages (~1.0–0.4 Ga) of the Bayan Obo deposit.

Xiao et al. [74] indicated that there are distinct differences between the Bayan Obo Group on the northern and southern sides of the Baiyinjiaolake–Kuangou–Ulanbaolige fault. To the south, the rocks of the Bayan Obo Group unconformably onlap the Wutai Group. To the north, it forms the continental margin subduction–accretionary complex belts on the northern edge of the NCC, which have been strongly deformed and dismembered by repeated subduction and collisions during the late stages of the PAO. Subduction and collision of the PAO plate with the NCC resulted in multistage tectonic–thermal events, especially from ~520 to ~380 Ma [52,75], which are consistent with the peak age (~0.5–0.4 Ga) of the Bayan Obo deposit.

In the Bayan Obo deposit, all the dominant Th–Pb-bearing minerals accumulated abundant radiogenic  $^{208}\text{Pb}$  since their formation in the Mesoproterozoic [5,76]. According to the Pb isotopic research of Chen et al. [7], during this Early Paleozoic metasomatic event, radiogenic  $^{208}\text{Pb}$  could have been mobilized and possibly released from the REE-bearing monazite and bastnasite. The anomalous, highly radiogenic  $^{208}\text{Pb}/^{204}\text{Pb}$  signatures in dolomite suggest the incorporation of thorogenic  $^{208}\text{Pb}$  during the Early Paleozoic [7].

The U–Th–Pb system of monazite behaves differently depending on the deformation mechanism—dissolution precipitation creep or dislocation creep—activated in the hosting metamorphic rocks [20]. The multistage tectonic–thermal event of ~1.0–0.4 Ga resulted in the Bayan Obo deposit being intensely overprinted by fluid [1,6,9–11] and caused variable Pb loss [7,8,11]. A wide range in apparent, geologically inaccurate Th–Pb and U–Pb ages among the patchy zones is the result of incomplete removal of in situ-grown radiogenic Pb from the patchy domains, depletion of Th and U, and the redistribution of Th and U among the domains [20]. In sample B-2, the in situ  $^{206}\text{Pb}$  ages of monazites show old cores and new rims. According to Wawrzenitz et al. [20] the cores of monazite are patchy, reflecting intra-grain, coupled dissolution–reprecipitation replacement processes. Exclusively in the rims of the old monazite, the chemical composition correlates to that of the syndeformative monazites, and the U–Th–Pb system reflects the subsequent creep or dislocation creep [20], this may be one of the reasons why the age span of monazite in the Bayan Obo deposit is so large.

Moreover, the peak ages of monazite from the dikes and orebody are ~1.3–0.8 Ga and ~0.5–0.4 Ga, respectively. There was as much as a 40% loss of  $\text{CO}_2$  from the precursor dolomite, although most of the recrystallized dolomite experienced decarbonation on a smaller scale [11]. The numerous ages of monazite, such as  $621 \pm 28$  Ma,  $763 \pm 16$  Ma and  $689 \pm 22$  Ma in this paper, may represent the separate thermal events and the partial recrystallization of monazite.

The Sm–Nd dating using the minerals, including huanghoite and rubidium–strontium dating using single-grain biotites, both from the later veins, shows concordant isochrons corresponding to  $442 \pm 42$  Ma and  $459 \pm 41$  Ma, respectively [50]. The Ar–Ar ages of riebeckite in veins cutting the H8 dolomite in the ore bodies show  $389.5 \pm 3.0$  Ma [21]. The Re–Os of pyrite from a vein cutting REE mineralization yield an isochron age of  $439 \pm 86$  Ma [52]. The three methods of Sm–Nd, Ar–Ar, and Re–Os of different minerals all recorded the Paleozoic tectonic–thermal event accompanied by a hydrothermal fluid event associated with the PAO. The Paleozoic tectonic–thermal event may generate a second phase of REE–Nb mineralization [21,50]. However, it is controversial whether the second REE mineralization occurred during this period. According to the new research on pyrite from Zhang et al. [10], the Paleozoic thermal events contributed little to the primary REEs mineralization except remobilizing pre-existing ore metals. Both the samples of Fe-1 and B-2 contain pyrite which likely formed at ~0.4 Ga; but the two samples also contain monazites that range from 1393–429 Ma and 818–597 Ma, respectively. So, the numerous Paleozoic monazites in previous research maybe be attributed to the restarting of the closure system due to the high temperature associated with the PAO. Additionally, some minerals, such as aegirine, aegirine–augite, riebeckite, and pyrite are likely produced in the Paleozoic, so the Sm–Nd, Ar–Ar, and Re–Os dating of minerals or ores will produce the Paleozoic age.

### 6.7.5. ~0.3–0.2 Ga

Most of the ~0.3–0.2 Ga period is accounted for by the U–Pb zircon ages of granitoids near the Bayan Obo deposit. The granites formed during the post-collisional tectonic regime due to closure of the PAO. This tectonic-thermal event only recorded the time of the disturbance, not the mineralization age of the Bayan Obo deposit [25,52,77].

## 7. Conclusions

(1) The monazite in the ore body samples yielded three  $^{207}\text{Pb}$  intercept ages of  $657 \pm 25$  Ma (MSWD = 1.06),  $763 \pm 16$  Ma (MSWD = 1.3), and  $689 \pm 22$  Ma (MSWD = 8.1), and the ages ranged from  $1393 \pm 142$  Ma to  $429 \pm 24$  Ma in one section.

(2) The earliest and major stages of carbonatites, REE, and dikes in the Bayan Obo deposit area are ~1.4 Ga and ~1.3 Ga, respectively, which are related to the breakup of Columbia.

(3) The multiple or protracted isotopic dates in the Bayan Obo deposit range from ~1.4–0.4 Ga due to five reasons: First, the separate thermal events and the partial recrystallization of monazite. Second, the diffusion of daughter products from the host mineral over time, such as Pb loss. Third, differences in the closure temperatures of different minerals and isotopic chronologies. Four, resetting of the closure system due to high temperature and hydrothermal alteration. Five, the minerals and transformed ores that formed at Paleozoic.

**Author Contributions:** Conceptualization, P.T., X.Y., Y.X. and W.Y.; investigation, P.T. and X.Y.; funding acquisition, P.T. and X.Y.; project administration, X.Y.; writing—original draft preparation, P.T.; writing—review and editing, P.T., X.Y. and W.Y.; visualization, Y.X. and Z.H. All authors have read and agreed to the published version of the manuscript.

**Funding:** This study is supported by the Key Research Program of the Chinese Academy of Sciences (Grant No. ZDRW-CN-2021-3); The Science and Technology Funding Project of Shanxi Institute of Engineering and Technology (No. 2021QD-21); and The Outstanding Doctoral Funding Project for Work in Shanxi (No. 2022PT-03).

**Data Availability Statement:** The data are presented directly in the present study.

**Acknowledgments:** We are grateful to four anonymous reviewers for providing valuable comments on an earlier version of this paper and F.Y. Wang and Q.Y. Yuan for valuable suggestions. Thanks to Y.S. Ren and J.Y. Cao for the field trip.

**Conflicts of Interest:** The authors declare no conflict of interest.

## References

1. Yang, K.F.; Fan, H.R.; Pirajno, F.; Li, X.C. The Bayan Obo (China) giant REE accumulation conundrum elucidated by intense magmatic differentiation of carbonatite. *Geology* **2019**, *47*, 1198–1202. [[CrossRef](#)]
2. Yang, X.Y.; Lai, X.D.; Pirajno, F.; Liu, Y.; Ling, M.X.; Sun, W.D. Genesis of the Bayan Obo Fe-REE-Nb formation in Inner Mongolia, North China Craton: A perspective review. *Precambrian Res.* **2017**, *288*, 39–71. [[CrossRef](#)]
3. Fan, H.R.; Hu, F.F.; Yang, K.F.; Pirajno, F.; Liu, X.; Wang, K.Y. Integrated U–Pb and Sm–Nd geochronology for a REE-rich carbonatite dyke at the giant Bayan Obo REE deposit, Northern China. *Ore Geol. Rev.* **2014**, *63*, 510–519. [[CrossRef](#)]
4. Tian, P.F.; Yang, X.Y.; Yuan, W.M. Formation and preservation of the Bayan Obo Fe-REE-Nb deposit, Inner Mongolia: Insights from evidences of petrogenesis, geochemistry and apatite fission track dating. *Solid Earth Sci.* **2021**, *6*, 228–245. [[CrossRef](#)]
5. Zhu, X.K.; Sun, J.; Pan, C.X. Sm–Nd isotopic constraints on rare-earth mineralization in the Bayan Obo ore deposit, Inner Mongolia, China. *Ore Geol. Rev.* **2015**, *64*, 543–553. [[CrossRef](#)]
6. Song, W.L.; Xu, C.; Smith, M.P.; Chakhmouradian, A.R.; Brenna, M.; Kynický, J.; Chen, W.; Yang, Y.H.; Deng, M.; Tang, H.Y. Genesis of the world's largest rare earth element deposit, Bayan Obo, China: Protracted mineralization evolution over ~1 b.y. *Geology* **2018**, *46*, 323–326. [[CrossRef](#)]
7. Chen, W.; Liu, H.Y.; Lu, J.; Jiang, S.Y.; Simonetti, A.; Xu, C.; Zhang, W. The formation of the ore-bearing dolomite marble from the giant Bayan Obo REE-Nb-Fe deposit, Inner Mongolia: Insights from micron-scale geochemical data. *Miner. Depos.* **2019**, *55*, 131–146. [[CrossRef](#)]
8. Li, X.C.; Yang, K.F.; Spandler, C.; Fan, H.R.; Zhou, M.F.; Hao, J.L.; Yang, Y.H. The effect of fluid-aided modification on the Sm–Nd and Th–Pb geochronology of monazite and bastnäsite: Implication for resolving complex isotopic age data in REE ore systems. *Geochim. Cosmochim. Acta* **2021**, *300*, 1–24. [[CrossRef](#)]

9. Li, H.T.; Yang, K.F.; Gao, Y.P.; Zhao, J.; Yuan, X.Y.; Li, X.C.; Fan, H.R. Age and origin of the H9 member from the Bayan Obo Group: Implications for the genesis of the giant Bayan Obo Fe-Nb-REE deposit, China. *Ore Geol. Rev.* **2022**, *146*, 104927. [[CrossRef](#)]
10. She, H.D.; Fan, H.R.; Yang, K.F.; Liu, X.; Li, X.H.; Dai, Z.H. Carbonatitic footprints in the Bayan Obo REEs deposit as seen from pyrite geochemistry. *Precambrian Res.* **2022**, *379*, 106801. [[CrossRef](#)]
11. Wei, C.W.; Deng, M.; Xu, C.; Chakhmouradian, A.R.; Smith, M.P.; Kynicky, J.; Song, W.L.; Chen, W.; Fu, B. Mineralization of the Bayan Obo Rare Earth Element Deposit by Recrystallization and Decarbonation. *Econ. Geol.* **2022**, *117*, 1327–1338. [[CrossRef](#)]
12. Tang, H.; Liu, Y.; Song, W. Igneous genesis of the Bayan Obo REE–Nb–Fe deposit: New petrographical and structural evidence from the H1–H9 cross-section and deep-drilling exploration. *Ore Geol. Rev.* **2021**, *138*, 104397. [[CrossRef](#)]
13. Fan, H.R.; Yang, K.F.; Hu, F.F.; Liu, S.; Wang, K.Y. The giant Bayan Obo REE–Nb–Fe deposit, China: Controversy and ore genesis. *Geosci. Front.* **2016**, *7*, 335–344. [[CrossRef](#)]
14. Smith, M.P.; Campbell, L.S.; Kynicky, J. A review of the genesis of the world class Bayan Obo Fe–REE–Nb deposits, Inner Mongolia, China: Multistage processes and outstanding questions. *Ore Geol. Rev.* **2015**, *64*, 459–476. [[CrossRef](#)]
15. Chew, D.; Spikings, R. Geochronology and Thermochronology Using Apatite: Time and Temperature, Lower Crust to Surface. *Elements* **2015**, *11*, 189–194. [[CrossRef](#)]
16. Danišik, M. Integration of fission-track thermochronology with other geochronologic methods on single crystals. In *Fission-Track Thermochronology and Its Application to Geology*; Springer International Publishing: Cham, Switzerland, 2019; pp. 93–108. Available online: <https://www.springer.com/series/15201> (accessed on 25 September 2022).
17. Liu, Y.L.; Chen, J.F.; Li, H.M.; Qian, H.; Xiao, G.W.; Zhang, T.R. Single-grain U–Th–Pb–Sm–Nd dating of monazite from dolomite type ore of the Bayan Obo, deposit. *Acta Petrol. Sin.* **2005**, *21*, 881–888. (In Chinese)
18. Smith, H.A.; Giletti, B.J. Lead diffusion in monazite. *Geochim. Cosmochim. Acta* **1997**, *61*, 1047–1055. [[CrossRef](#)]
19. Cherniak, D.; Watson, E.B.; Grove, M.; Harrison, T.M. Pb diffusion in monazite: A combined RBS/SIMS study. *Geochim. Cosmochim. Acta* **2004**, *68*, 829–840. [[CrossRef](#)]
20. Wawrzenitz, N.; Krohe, A.; Rhede, D.; Romer, R.L. Dating rock deformation with monazite: The impact of dissolution precipitation creep. *Lithos* **2012**, *134*, 52–74. [[CrossRef](#)]
21. Lai, X.D.; Yang, X.Y.; Santosh, M.; Liu, Y.L.; Ling, M.X. New data of the Bayan Obo Fe–REE–Nb deposit, Inner Mongolia: Implications for ore genesis. *Precambrian Res.* **2015**, *263*, 108–122. [[CrossRef](#)]
22. Ren, Y.S.; Yang, X.Y.; Wang, S.S.; Öztürk, H. Mineralogical and geochemical study of apatite and dolomite from the Bayan Obo giant Fe–REE–Nb deposit in Inner Mongolia: New evidences for genesis. *Ore Geol. Rev.* **2019**, *109*, 381–406. [[CrossRef](#)]
23. Santosh, M. Assembling North China Craton within the Columbia supercontinent: The role of double-sided subduction. *Precambrian Res.* **2010**, *178*, 149–167. [[CrossRef](#)]
24. IGCAS. *Geochemistry of the Bayan Obo Deposit*; Science Press: Beijing, China, 1988. (In Chinese)
25. Ling, M.X.; Zhang, H.; Li, H.; Liu, Y.L.; Liu, J.; Li, L.Q.; Li, C.Y.; Yang, X.Y.; Sun, W.D. The Permian–Triassic granitoids in Bayan Obo, North China Craton: A geochemical and geochronological study. *Lithos* **2014**, *190–191*, 430–439. [[CrossRef](#)]
26. Kusky, T.; Li, J.; Santosh, M. The Paleoproterozoic North Hebei orogen: North China craton’s collisional suture with the Columbia supercontinent. *Gondwana Res.* **2007**, *12*, 4–28. [[CrossRef](#)]
27. Zhong, Y.; Zhai, M.; Peng, P.; Santosh, M.; Ma, X. Detrital zircon U–Pb dating and whole-rock geochemistry from the clastic rocks in the northern marginal basin of the North China Craton: Constraints on depositional age and provenance of the Bayan Obo Group. *Precambrian Res.* **2015**, *258*, 133–145. [[CrossRef](#)]
28. Liu, Y.F.; Bagas, L.; Nie, F.J.; Jiang, S.H.; Li, C. Re–Os system of black schist from the Mesoproterozoic Bayan Obo Group, Central Inner Mongolia, China and its geological implications. *Lithos* **2016**, *261*, 296–306. [[CrossRef](#)]
29. Ning, S.Y.; Wang, F.Y.; Xue, W.D.; Zhou, T.F. Geochemistry of the Baoshan pluton in the Tongling region of the Lower Yangtze River Belt. *Geochimica* **2017**, *46*, 397–412.
30. Wang, F.Y.; Ge, G.; Ning, S.Y.; Nie, L.Q.; Zhong, G.X.; White, N.C. A new approach to LA-ICP-MS mapping and application in geology. *Acta Petrol. Sin.* **2017**, *33*, 3422–3436. (In Chinese)
31. Gonçalves, G.O.; Lana, C.; Scholz, R.; Buick, I.S.; Gerdes, A.; Kamo, S.L.; Corfu, F.; Marinho, M.M.; Chaves, A.O.; Valeriano, C. An assessment of monazite from the Itambé pegmatite district for use as U–Pb isotope reference material for microanalysis and implications for the origin of the “Moacyr” monazite. *Chem. Geol.* **2016**, *424*, 30–50. [[CrossRef](#)]
32. Ling, X.X.; Huyskens, M.H.; Li, Q.L.; Yin, Q.Z.; Werner, R.; Liu, Y.; Tang, G.Q.; Yang, Y.N.; Li, X.H. Monazite RW-1: A homogenous natural reference material for SIMS U–Pb and Th–Pb isotopic analysis. *Mineral. Petrol.* **2017**, *111*, 163–172. [[CrossRef](#)]
33. Ludwig, K.R. *Isoplot 3.00: A Geochronological Toolkit for Microsoft Excel*; No. 4; Berkeley Geochronology Center Special Publication: Berkeley, CA, USA, 2003; 74p.
34. Zhang, Z.Q.; Yuan, Z.X.; Tang, S.H.; Bai, G.; Wang, J.H. *Age and Geochemistry of the Bayan Obo Ore Deposit*; Geological Publishing House: Beijing, China, 2003. (In Chinese)
35. Fan, H.R.; Yang, K.F.; Hu, F.F.; Wang, K.Y.; Zhai, M.G. Zircon geochronology of basement rocks from the Bayan Obo area, Inner Mongolia, and tectonic implications. *Acta Petrol. Sin.* **2010**, *26*, 1342–1350. (In Chinese)
36. Wang, K.Y.; Fan, H.R.; Xie, Y.H.; Li, H.M. Zircon U–Pb dating of basement gneisses in the super-large Bayan Obo REE–Fe–Nb deposit, Inner Mongolia. *Chin. Sci. Bull.* **2002**, *47*, 245–248. (In Chinese)
37. Liu, Y.L.; Ling, M.X.; Williams, I.S.; Yang, X.Y.; Wang, C.Y.; Sun, W.D. The formation of the giant Bayan Obo REE–Nb–Fe deposit, North China, Mesoproterozoic carbonatite and overprinted Paleozoic dolomitization. *Ore Geol. Rev.* **2018**, *92*, 73–83. [[CrossRef](#)]

38. Fan, H.R.; Chen, F.K.; Wang, K.Y.; Xie, Y.H.; Wilde, S.; Stair, M. Zircon U-Pb age of a carbonatite dyke from Bayan Obo REE-Fe-Nb deposit, Inner Mongolia and its geological significance. *Acta Petrol. Sin.* **2002**, *18*, 363–368. (In Chinese)
39. Lai, X.D.; Yang, X.Y. U-Pb Ages and Hf Isotope of Zircons from a Carbonatite Dyke in the Bayan Obo Fe-REE Deposit in Inner Mongolia: Its Geological Significance. *Acta Geol. Sin.* **2019**, *93*, 1783–1796. [[CrossRef](#)]
40. Liu, Y.L.; Williams, I.S.; Chen, J.F.; Wan, Y.S.; Sun, W.D. The significance of Paleoproterozoic zircon in carbonatite dikes associated with the Bayan Obo REE-Nb-Fe deposit. *Am. J. Sci.* **2008**, *308*, 379–397. [[CrossRef](#)]
41. Fan, H.R.; Hu, F.F.; Chen, F.K.; Yang, K.F.; Wang, K.Y. Intrusive age of No. 1 carbonatite dyke from Bayan Obo REE-Nb-Fe deposit, Inner Mongolia: With answers to comment of Dr. Le Bas. *Acta Petrol. Sin.* **2006**, *22*, 519–520. (In Chinese)
42. Liu, Y.L.; Chen, J.F.; Li, H.M.; Xiao, G.W.; Zhang, T.R. Geochronology of the carbonatite dykes in the Bayan Obo orefield. *Revisit. Geol. Rev.* **2006**, *52*, 415–422.
43. Ni, P.; Zhou, J.; Chi, Z.; Pan, J.Y.; Li, S.N.; Ding, J.Y.; Han, L. Carbonatite dyke and related REE mineralization in the Bayan Obo REE ore field, North China: Evidence from geochemistry, CO isotopes and RbSr dating. *J. Geochem. Explor.* **2020**, *215*, 106560. [[CrossRef](#)]
44. Yang, K.F.; Fan, H.R.; Santosh, M.; Hu, F.F.; Wang, K.Y. Mesoproterozoic carbonatitic magmatism in the Bayan Obo deposit, Inner Mongolia, North China: Constraints for the mechanism of super accumulation of rare earth elements. *Ore Geol. Rev.* **2011**, *40*, 122–131. [[CrossRef](#)]
45. Wang, J.; Cheng, Z.; Gui, X. Rb-Sr isotopic characteristics of granitic rocks from Bayan Obo, Nei Mongol, China. *Ann. Rep. 1982-I 983 Inst. Geochem. Acad. Sin.* **1983**.
46. Ling, M.X.; Liu, Y.L.; Williams, I.S.; Teng, F.Z.; Yang, X.Y.; Ding, X.; Wei, G.J.; Xie, L.H.; Deng, W.F.; Sun, W.D. Formation of the world's largest REE deposit through protracted fluxing of carbonatite by subduction-derived fluids. *Sci. Rep.* **2013**, *3*, 1776. [[CrossRef](#)]
47. Fan, H.R.; Hu, F.F.; Yang, K.F.; Wang, K.Y.; Liu, Y.S. Geochronology framework of late Paleozoic dioritic-granitic plutons in the Bayan Obo area, Inner Mongolia, and tectonic significance. *Acta Petrol. Sin.* **2009**, *25*, 2933–2938. (In Chinese)
48. Zhang, Z.Q.; Tang, S.S.; Chen, Q.T.; Wang, J.H. Sm-Nd Ages and Origins of Metamorphic Rocks for the H9 Formation in the Bayan Obo Ore District, and Relationship with the Ore Forming Event. *Acta Geosci. Sin.* **1997**, *18*, 267–274. (In Chinese)
49. Khain, E.V.; Bibikova, E.V.; Salnikova, E.B.; Kröner, A.; Gibsher, A.S.; Didenko, A.N.; Degtyarev, K.E.; Fedotova, A.A. The Palaeo-Asian ocean in the Neoproterozoic and early Palaeozoic: New geochronologic data and palaeotectonic reconstructions. *Precambrian Res.* **2003**, *122*, 329–358. [[CrossRef](#)]
50. Hu, F.F.; Fan, H.R.; Liu, S.; Yang, K.F.; Chen, F.K. Samarium–Neodymium and Rubidium–Strontium Isotopic Dating of Veined REE Mineralization for the Bayan Obo REE-Nb-Fe Deposit, Northern China. *Resour. Geol.* **2009**, *59*, 407–414. [[CrossRef](#)]
51. Zhang, Z.Q.; Tang, S.H.; Wang, J.H.; Yuang, Z.X.; Bai, G. Information about ore deposit formation in different epochs: Age of the west orebodies of the Bayan Obo deposit with a discussion. *Geol. China* **2003**, *30*, 130–137. (In Chinese)
52. Liu, Y.L.; Yang, G.; Chen, J.F.; Du, A.D.; Xie, Z. Re-Os dating of pyrite from Giant Bayan Obo REE-Nb-Fe deposit. *Chin. Sci. Bull.* **2004**, *49*, 2627–2631. [[CrossRef](#)]
53. Liu, L.S. The Re-Os isotopic age of molybdenite from Bayan Obo REE ore deposit. *Min. Depos.* **1996**, *15*, 188–191. (In Chinese)
54. Ren, Y.C.; Zhang, Y.C.; Zhang, Z.Q. Study on heat events of ore-forming Bayan Obo deposit. *Acta Geosci. Sin.* **1994**, *1–2*, 95–101. (In Chinese)
55. Wang, J.; Tatsumoto, M.; Li, X.; Premo, W.R.; Chao, E.C.T. A precise  $^{232}\text{Th}$ - $^{208}\text{Pb}$  chronology of fine-grained monazite: Age of the Bayan Obo REE-Fe-Nb ore deposit, China. *Geochim. Cosmochim. Acta* **1994**, *58*, 3155–3169. [[CrossRef](#)]
56. Chao, E.C.T.; Back, J.M.; Minkin, J.A.; Tatsumoto, M.; Junwen, W.; Conrad, I.E.; McKee, E.H.; Zonglin, H.; Qingrun, M.; Shengguang, H. *The Sedimentary Carbonate-Hosted Giant Bayan Obo REE-Fe-Nb Ore Deposit of Inner Mongolia, China: A Cornerstone Example for Giant Polymetallic Ore Deposits of Hydrothermal Origin*; US Government Printing Office: Washington, DC, USA, 1997; pp. 1–65.
57. Campbell, L.S.; Compston, W.; Sircombe, K.N.; Wilkinson, C.C. Zircon from the East Orebody of the Bayan Obo Fe–Nb–REE deposit, China, and SHRIMP ages for carbonatite-related magmatism and REE mineralization events. *Contrib. Mineral. Petrol.* **2014**, *168*, 1041. [[CrossRef](#)]
58. Zhang, S.H.; Zhao, Y.; Liu, Y.S. A precise zircon Th-Pb age of carbonatite sills from the world's largest Bayan Obo deposit: Implications for timing and genesis of REE-Nb mineralization. *Precambrian Res.* **2017**, *291*, 202–219. [[CrossRef](#)]
59. Yuan, Z.X.; Bai, G.; Zhang, Z.Q. Trachytic Rock and Associated Fenitization in the Bayan Obo Ore Deposit, Inner Mongolia, China: Evidence for Magmatic-Hydrothermal Mineralization Related to a Carbonatitic Complex. *Acta Geol. Sin.* **2000**, *74*, 148–153.
60. Zhang, Z.Q.; Tang, S.H.; Yuan, Z.X.; Bai, G.; Wang, J.H. The Sm-Nd and Rb-Sr isotopic systems of the dolomites in the Bayan Obo ore deposit, Inner Mongolia, China. *Acta Petrol. Sin.* **2001**, *17*, 637–642. (In Chinese)
61. Liu, S.; Fan, H.R.; Yang, K.F.; Hu, F.F.; Wang, K.Y.; Chen, F.K.; Yang, Y.H.; Yang, Z.F.; Wang, Q.W. Mesoproterozoic and Paleozoic hydrothermal metasomatism in the giant Bayan Obo REE-Nb-Fe deposit: Constrains from trace elements and Sr-Nd isotope of fluorite and preliminary thermodynamic calculation. *Precambrian Res.* **2018**, *311*, 228–246. [[CrossRef](#)]
62. Zhai, M.G.; Zhao, L.; Zhu, X.Y.; Zhou, Y.Y.; Peng, P.; Guo, J.H.; Li, Q.; Zhao, T.P.; Lu, J.S.; Li, X.H. Late Neoproterozoic magmatic–metamorphic event and crustal stabilization in the North China Craton. *Am. J. Sci.* **2021**, *321*, 206–234. [[CrossRef](#)]
63. Liu, F.; Guo, J.H.; Peng, P.; Qian, Q. Zircon U–Pb ages and geochemistry of the Huai'an TTG gneisses terrane: Petrogenesis and implications for ~2.5Ga crustal growth in the North China Craton. *Precambrian Res.* **2012**, *212–213*, 225–244. [[CrossRef](#)]

64. Polat, A.; Herzberg, C.; Münker, C.; Rodgers, R.; Kusky, T.; Li, J.; Fryer, B.; Delaney, J. Geochemical and petrological evidence for a suprasubduction zone origin of Neoproterozoic (ca. 2.5 Ga) peridotites, central orogenic belt, North China craton. *GSA Bull.* **2006**, *118*, 771–784. [[CrossRef](#)]
65. Diwu, C.R.; Sun, Y.; Guo, A.L.; Wang, H.L.; Liu, X.M. Crustal growth in the North China Craton at ~2.5Ga: Evidence from in situ zircon U–Pb ages, Hf isotopes and whole-rock geochemistry of the Dengfeng complex. *Gondwana Res.* **2011**, *20*, 149–170. [[CrossRef](#)]
66. Zhao, G.C. Metamorphic evolution of major tectonic units in the basement of the North China Craton: Key issues and discussion. *Acta Petrol. Sin.* **2009**, *25*, 1772–1792. (In Chinese)
67. Zhao, G.C.; Sun, M.; Wilde, S.A.; Li, S.Z. Late Archean to Paleoproterozoic evolution of the North China Craton: Key issues revisited. *Precambrian Res.* **2005**, *136*, 177–202. [[CrossRef](#)]
68. Zhao, G.C.; Wilde, S.A.; Sun, M.; Guo, J.H.; Kröner, A.; Li, S.Z.; Li, X.P.; Zhang, J. SHRIMP U–Pb zircon geochronology of the Huai’an Complex: Constraints on Late Archean to Paleoproterozoic magmatic and metamorphic events in the Trans-North China Orogen. *Am. J. Sci.* **2008**, *308*, 270–303. [[CrossRef](#)]
69. Trap, P.; Faure, M.; Lin, W.; Bruguier, O.; Monié, P. Contrasted tectonic styles for the Paleoproterozoic evolution of the North China Craton. Evidence for a ~2.1 Ga thermal and tectonic event in the Fuping Massif. *J. Struct. Geol.* **2008**, *30*, 1109–1125. [[CrossRef](#)]
70. Trap, P.; Faure, M.; Lin, W.; Monié, P. Late Paleoproterozoic (1900–1800 Ma) nappe stacking and polyphase deformation in the Hengshan–Wutaishan area: Implications for the understanding of the Trans-North-China Belt, North China Craton. *Precambrian Res.* **2007**, *156*, 85–106. [[CrossRef](#)]
71. Zhao, G.C.; Li, S.Z.; Sun, M.; Wilde, S.A. Assembly, accretion, and break-up of the Palaeo-Mesoproterozoic Columbia supercontinent: Record in the North China Craton revisited. *Int. Geol. Rev.* **2011**, *53*, 1331–1356. [[CrossRef](#)]
72. Zhao, G.C.; Sun, M.; Wilde, S.A.; Li, S.Z. Assembly, accretion and breakup of the Paleo-Mesoproterozoic Columbia Supercontinent: Records in the North China Craton. *Gondwana Res.* **2003**, *6*, 417–434. [[CrossRef](#)]
73. Rogers, J.J.; Santosh, M. Tectonics and surface effects of the supercontinent Columbia. *Gondwana Res.* **2009**, *15*, 373–380. [[CrossRef](#)]
74. Xiao, Q.H.; Liu, Y.; Xu, L.Q.; Ding, X.Z.; Zhang, Y.Q.; Cheng, Y.; Li, Y.; Fan, Y.X.; He, G.Q. Preliminary Study on Geology and Mineralization of the Bayan Obo Ocean Plate. *Earth Sci.* **2020**, *45*, 2258–2278. (In Chinese)
75. Zhang, S.H.; Zhao, Y.; Ye, H.; Liu, J.M.; Hu, Z.C. Origin and evolution of the Bainaimiao arc belt: Implications for crustal growth in the southern Central Asian orogenic belt. *Bulletin* **2014**, *126*, 1275–1300. [[CrossRef](#)]
76. Zhang, S.H.; Zhao, Y.; Li, Q.L.; Hu, Z.C.; Chen, Z.Y. First identification of baddeleyite related/linked to contact metamorphism from carbonatites in the world’s largest REE deposit, Bayan Obo in North China Craton. *Lithos* **2017**, *284*, 654–665. [[CrossRef](#)]
77. Yang, K.F.; Fan, H.; Hu, F.F.; Li, X.H.; Liu, J.Y.; Zhao, Y.G.; Liu, S.; Wang, K.Y. Skarnization age in the giant Bayan Obo REE-Nb-Fe ore district, Inner Mongolia, China: Rb-Sr isochrone dating on single-grain phlogopite. *Acta Petrol. Sin.* **2007**, *23*, 1018–1022. (In Chinese)